1-1-2007

Enhancement of root crack detection in friction stir welds using ultrasonic non-destructive testing and signal processing technique.

Kathleen Dizon
University of Windsor

NOTE TO USERS

This reproduction is the best copy available.

UMI ®

Enhancement of Root Crack Detection in Friction Stir Welds Using Ultrasonic Non-destructive Testing And Signal Processing Technique

by
Kathleen Dizon

A Thesis
Submitted to the Faculty of Graduate Studies
through Electrical and Computer Engineering Department
in Partial Fulfillment of the Requirements for
the Degree of Master of Science at the
University of Windsor

Windsor, Ontario, Canada
2007
© 2007 Kathleen Dizon

Canada

ABSTRACT

The role and scope of non-destructive evaluation (NDE) is continuously changing over time in order to meet the emerging challenges concomitant with new materials and process technologies. Among these are the new inspection methods required by new advanced technologies, such as NDE for the analysis of friction stir welds (FSW) in quality control applications. Recent increases in the industrial application of FSW to join materials that are difficult to fusion weld, has intensified the need for a non-destructive technique to detect and characterize defects that may occur in products produced by FSW. The challenge to meeting this need arises from the tendency of these defects to be very tight and very small, and that they may occur at any orientation. This wide variety of defect orientations is very unusual for conventional weld inspection, and their small, tight geometry adds to the challenge. In this thesis, we compared the sensitivity of several non-destructive methods to determine the optimal approach. Analyses of A-scan signals, experimentation with phased array probes and single element probes were used to test the detection of cracks in FSW. The improvement of detection was verified experimentally on aluminum samples with simulated flaws. Consequently, with some limitations of ultrasonic testing in detecting micro cracks, signal processing technique was applied. Noise suppression of A-scans was done by utilizing wavelet transform. Enhancements of ultrasonic signals were based by the significant increase in signal to noise ratio.

DEDICATION

To God, to my parents, to my sisters

iv

ACKNOWLEDGEMENTS

I am deeply grateful to many people for their support not only through writing this paper but also throughout my entire Master's Degree campaign. I sincerely thank my supervisor, Dr. Roman Maev, for his continuous support and guidance, for all the opportunities and for all the knowledge I earned by listening to his advices.

Further, the members of Dr. Maev's group have provided both encouragement and assistance. Especially, I would like to say thank you to Dr. Sergey Titov for his help since the beginning of my journey. For all the suggestions, comments and even advices that help me finish this thesis. Also, thanks to other members, Dr. Severyn and Ms. Sarah Beneteau.

The role of Dr. Ahmadi, Dr. Kedzierski and Dr. Sid-Ahmed as my committee members is also greatly appreciated. The careful examination of this paper along with their constructive evaluation was very beneficial.

And finally, I would like to thank my family, here in Windsor and back home in the Philippines. Thanks to my mama and papa and kambal for continuously praying for my success. Thanks to my lolo and lola for guiding me to make the right decisions. I will always be grateful for their loving support and inspiration. Finally, thanks to God Almighty.

v

TABLE OF CONTENTS

SIGNAL PROCESSING TO ENHANCE DEFECT DETECTION

CONCLUSION AND FUTURE WORKS

vii

LIST OF TABLES

LIST OF FIGURES

x

CHAPTER I

INTRODUCTION

Nondestructive Testing (NDT) is a very broad field that performs a vital role in assuring that structural components and systems are in good condition and functions very well as they were expected. The tests are performed in an approach that does not affect the future worth of the components being examined. Shortly, NDT allows materials to be inspected and measured without damaging the materials themselves. In this manner, it provides a balance between quality control and cost, which in turn is very valuable for industrial companies. Even though NDT has been useful in the industry for the past few decades, the role and scope of NDT is continuously changing over time in order to meet the emerging challenges concomitant with new materials and process technologies. Among these are some new inspection trends for the analysis of friction stir welds (FSW) in quality control applications. Recent increases in the industrial application of FSW to join materials that are difficult to fusion weld, has intensified the need for a nondestructive technique to detect and characterize defects that may occur on its products. The challenge to meeting this need arises from the tendency of these defects to be very tight and very small, and that they may occur at any orientation. This wide variety of defect orientations is very unusual for conventional weld inspection, and their small, tight geometry adds to the challenge.

Friction stir welding technology is not that old. It was invented by The Welding Institute in Cambridge in December 1991 and the Lockheed Martin began its development activities in 1995. FSW development continued at Marshall Space Flight Center through 2001 for various NASA applications including man-rated flight hardware. Because of the continuous promising applications of FSW, specifically in aerospace industry, it brought about the need for a high-resolution, non-destructive testing technology to enhance its quality and reliability with benefits in cost production and human protection.

In 2002, the American Welding Society conducted several tests to explore friction stir welded materials (Kinchen and Aldahir, 2006). They worked on the 2XXX series aluminum alloys in their experiments and testing. This family of aluminum alloys

1

has long been used in aerospace production because of having high-strength and light-weight property. They have used several NDE techniques to compare results such as visual inspection, liquid penetrant testing, radiography and ultrasonic testing. With their output, they concluded that ultrasonic testing will replace the older types of testing and will greatly improve the detection performance in welded materials. This is when the utilization of ultrasonic testing in FSW begun. In 2004, Ontario Power Generation-Inspection Services Division, a group of experts, performed an examination on FSW steel bars with fatigue induced cracks using single element transducers and ultrasonic phased array probes. Their results showed that conventional probes could detect size cracks within 1.5mm accuracy while phased array probes were more reliable, detecting within 0.5mm accuracy (Ciorau, 2004). Also on the same year, RD Tech published a book entitled Introduction to Phased Array Ultrasonic Technology Applications. And in here, they have mentioned their results in their thorough study of friction stir welds. They have started this case study in the year 2000 by Andre Lamarre and Michael Moles. These people focused on possibility of detecting micro cracks that are present in FSW materials. Micro defects like wormholes, kissing bonds, lack of penetration, faying surface defects and root toe defects are given attention on this study.

In this thesis, more attention was given to the analysis and detection of root defects. These kinds of defects, even in other materials not made by FSW technology, are very crucial because it emerges along the weld root itself which causes stress concentration of the material (Connor, 1991). This affects the durability of the FSW. The major problem is it is not straightforward to detect these defects because it usually reflects a very small amount of amplitude compare with the noise and other background echoes. Isolation of reflections coming from this root crack among those background noises was done in order to conclude detection performance. Studies of sensitivity of several ultrasonic testing methods were implemented to determine the optimal approach. Analyses of A-scan signals, experimentation with phased array probes and single element probes were used to test the detection of cracks in FSW. The improvement of detection was verified experimentally on aluminum samples with simulated flaws. In addition, this thesis utilized the relevance of signal processing techniques to improve root crack detection. Discrete Wavelet Transform (DWT) was applied to the acquired ultrasonic

2

signal to increase signal-to-noise ratio for easier detectability of the small tight cracks. Determining the best mother wavelet that will correlate to the ultrasonic pulse echo was also investigated to provide the best SNR and resolution. And of course, the principles behind this inspection and signal enhancing were studied thoroughly.

Chapter 2 of this thesis will discuss deeply on the problems encounter in investigating FSW with conventional ultrasonic testing. The challenges of the FSW and limitations of ultrasonic testing will be given much importance. Also, the main goal of the project will be mentioned.

Chapter 3 will provide the literature review of the processes and technologies associated with this research. Among these are the methodology and uniqueness of friction stir welding including the creation of micro cracks; the ultrasonic nondestructive testing principles, the physics behind it and inspection trends.

Chapter 4 contains the author's first step to solve the problem. This chapter is involved with the optimization of the sensitivity of different ultrasonic system which includes the Scanning Acoustic Microscopy and Angled Beam Inspection (single element and phased array), the principles and experimental results.

Chapter 5 will be the alternative approach due to some negative outcome of the approach on previous chapter. This includes the utilization of different signal processing techniques used in flaw detection and finally the application of Wavelet Transform in the ultrasonic signals to improved detection of small cracks.

Conclusions on the conducted study will be stated in Chapter 6 together with a few recommendations for future studies in this field. This thesis will end up with some appendices that will provide further theories and principles useful in understanding the body of this research.

3

CHAPTER II

PROBLEM STATEMENTS AND OBJECTIVES

2.1. Problem Statement

The problems connected to ultrasonic testing of friction stir weldings were divided into two categories. First, the challenges of friction stir weld products itself, what makes FSW difficult to inspect nondestructively? Secondly, due to those challenges, it caused difficulties in signal interpretation.

There were few problems encountered during the inspection of FSW materials using the conventional way of ultrasonic nondestructive testing. Some of these are the following:

- Geometrical Consideration. The creation of severe roughness of the top surface and curve-like bump on the bottom surface which causes rigorous amount of aberration and attenuation and multiple bouncing of ultrasound. And reflections from these roughnesses are often stronger than the reflection from the defects.

- Metallurgical Changes. The change of the physical properties of the material due to frictional heat causes change in velocity and angle of refraction of ultrasound.

- Micro Cracks Generation. Generation of micro cracks in the material, such as root crack, that is very hard to detect because of small amount in amplitude and because of the nature of its orientation which is usually present vertically in FSWs.

4

Due to the encountered problems above, it causes the following difficulties in signal interpretation:

- It gives a very low signal-to-noise ratio.
- It lowers the precision of defect localization and sizing.
- It hides defect pulses from background noises.
- It gives difficulty on detection of crack appearance.
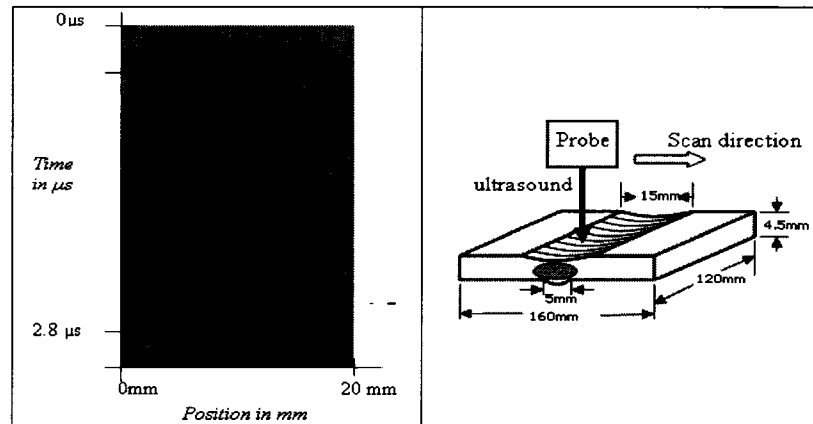
Figure 2.1 B-scan of FSW and inspection set-up and dimensions of the sample.

Left image on Figure 2.1 is a B-scan image of an FSW aluminum plate with a thickness of 4.5mm and the probe used was a focused Xatex immersion transducer with 20 MHz frequency and 1 inch focal distance. The image shows that using normal incidence ultrasound inspection would not be able to detect small cracks like root crack because of its nature of orientation. The B-scan only gives us profile of the FSW. Like mentioned on the above problems, the possible small reflections from this cracks might be negligible when overlapped with strong bottom signal and other background noise signals. In metals, many discontinuities are not flat or perpendicular to the incident sound beam and serve to scatter the ultrasonic energy. Such discontinuities show reduced echo signal levels in A-scans. Since root cracks are considered this kind of crack, normal incident inspection is not advisable. Further investigation with normal beam testing will be discussed on Chapter 4 with the investigation of FSW using Scanning Acoustic Microscopy.

5

2.2. Objectives of the Study

For the reason that the problem statement was divided into two categories, it will be adequate to have two categories of objectives as well but both coming up with the same main goal which is **to enhance or improve the detection of root cracks on FSW using UT-NDT**.

- First objective is to come up with the best ultrasonic inspection technology to inspect FSW.
  - o This includes discovering the system or method with the best sensitivity
  - o And determining the best parameters to apply in each method.
- Second, is to enhance the signals acquired to improve crack detection.
  - o This governs improvement of signal-to-noise ratio by suppressing noise in the acquired ultrasonic signals
  - o And by establishing the best possible mother wavelet to use in DWT noise suppression process.

Reproduced with permission of the copyright owner. Further reproduction prohibited without permission.

CHAPTER III

REVIEW OF RELATED LITERATURE

3.1. Friction Stir Welding

Since the invention of Friction Stir Welding (FSW) in the early 1990's, the process has received world-wide attention and was proven to be an efficient welding method for those materials that are difficult to weld using the conventional one. And up to the present times, researchers and experts are continuously searching for more applications and advantages of this emerging and promising welding technology.

3.1.1 Friction Stir Welding Technology

FSW is a vast development in welding industry. It was proven to provide resilient welds because of its unique welding procedure. A cylindrical shouldered tool with profiled pin is immersed into the junction of the metal plates to be joined. The cylindrical tool rotates with constant speed at the joint line while the plates are butted firmly. With this process, frictional heat is generated between the welding pin and the work piece. This heat causes the stirred material to soften but without reaching its melting point. This allows traversing of the tool on the weld line. The plasticized material is transferred from the leading edge of the tool to the trailing edge of the tool probe and is forged by the intimate contact of the tool shoulder and the pin profile. It leaves a solid phase bond between the two pieces. The process can be regarded as a solid phase keyhole welding technique since a hole to accommodate the probe is generated, then filled during the welding sequence (TWI, 2006).
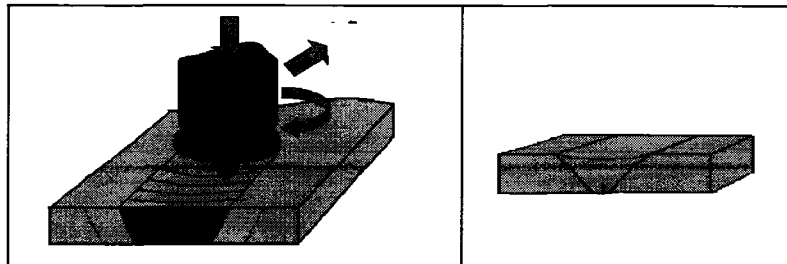
Figure 3.1.1 Friction stir welding technology and root crack.

7

The main advantage of this process is its ability to join materials in solid phase, not reaching their melting point. Means, it includes joining of materials that are difficult to weld using fusion welding. Examples are 2000 and 7000 aluminum alloys. The other secondary advantages but are still vital are the following:

1. Low distortion, even in long welds

2. Excellent mechanical properties as proven by fatigue, tensile and bend tests

3. No fumes, no porosity, no spatter

4. Low shrinkage, can operate in all positions, energy efficient

5. No grinding, brushing or pickling required in mass production

6. Can weld aluminum and copper of >50mm thickness in one pass.

Some of the limitations of FSW are now being studied by experts and researchers to look for a possible solution. However, the main disadvantages are:

1. Work pieces must be rigidly clamped

2. Backing bar required

3. Keyhole at the end of each weld

4. Cannot make joints which required metal deposition

FSW can be applied in different materials: aluminums, copper and its alloys, lead, titanium and its alloys, magnesium alloys, zinc, plastics, stainless steel and nickel alloys. Most of the typically used metals in industry are covered by its range that is why this process has been used in different fields and still being used because of the continuous discoveries of its effectiveness and advantages. Aerospace and marine industries are the first two applications of friction stir welding. The creation of panels for decks, sides, bulkheads and floors in marine spaces and other marine and transport structures are some of the aspects where FSW is superior. Wings, fuselages, empennages are also products of FSW in aeronautical field. The commercial production of high speed trains made from aluminum extrusions which may be joined by friction stir welding has also been published. The friction stir welding process is currently being used

8

commercially, and is also being assessed by several automotive companies and suppliers to this industrial sector for its commercial application. Existing and potential applications include engine and chassis cradles, wheel rims, truck bodies, buses and airfield transportation vehicles, motorcycle and bicycle frames, and a lot more to mention. Friction stir welding can also be considered for electric motor housings, refrigeration panels, cooking equipment and kitchens, white goods, gas tanks and gas cylinders, connecting of aluminum or copper coils in rolling mills and for making furniture. Since the scope of application of friction stir welding in dramatically increasing, the need for a better inspection to provide durable and reliable FSW product is necessary. The birth of cracks that makes FSW inspection difficult is talked about on the Section 3.1.2, together with the definition of root crack.

3.1.2. Creation of Cracks

width of tool shoulder
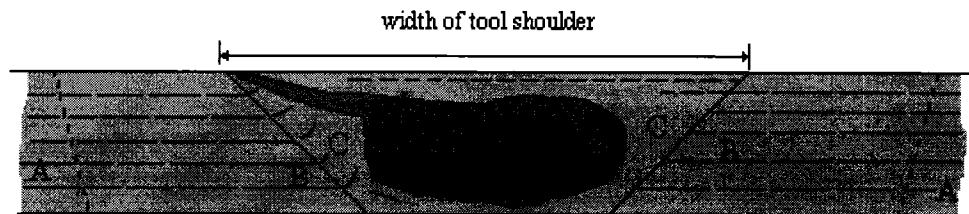
Figure 3.1.2 Metallurgical changes in FSW
(Figure from The Welding Institute Resources, "Friction Processes". Online. 2005)

A. Unaffected material

B. Heat affected zone (HAZ)

C. Thermo-mechanically affected zone (TMAZ)

D. Weld nugget (Part of thermo-mechanically affected zone)

Understanding the potential discontinuities for the FSW process requires an understanding of it metallurgy. The unaffected material or parent material is the part that is not deformed or altered and which although it may have

9

experienced a thermal cycle from the weld is not affected by the heat in terms of microstructure or mechanical properties. In heat affected zone region, which clearly will lie closer to the weld centre, the material has experienced a thermal cycle which has modified the microstructure and/or the mechanical properties. However, there is no plastic deformation occurring in this area. In TMAZ region, the material has been plastically deformed by the friction stir welding tool, and the heat from the process will also have exerted some influence on the material. In the case of aluminum, it is possible to get significant plastic strain without re-crystallization in this region, and there is generally a distinct boundary between the re-crystallized zone and the deformed zones of the TMAZ. The re-crystallized area in the TMAZ in aluminum alloys has traditionally been called the nugget. Refer to Figure 3.1.2 for the illustration of different zones. This microstructure classification has also been accepted by the Friction Stir Welding Licensees Association.

Due to the distinctive process, FSW has a tendency to create a variety of defects in the material. These wide varieties of defects are unusual for weld inspection because of their inclination to occur at any orientation and any angle, though in practice most defects tend to be axial or traverse (Lamarre et. al, 2000). Most of the defects occur at the butt weld portion and these are:

1. Lack of penetration
2. Wormholes
3. Kissing Bonds
4. Faying surface defects
5. Root toe defect

In this thesis, the focus of interest was mostly on the detection of root crack. It is very small in terms of crack depth, 50 to 90 μm and it is vertically oriented and located at the weld nugget of the material. For reference, see Figure 3.1.1.

10

3.1.3. Inspection of Friction Stir Welds

Several inspection methods have been used to analyze FSW composition, to determine some internal cracks and its durability. Some of the nondestructive inspection techniques that were already been used for analyzing FSWs will be briefly described, such as Visual Inspection, Liquid Penetrant Testing, Magnetic Particle, Radiography, and Eddy Current Testing. Consequently, the drawbacks and disadvantages of these processes will lead us to the motivation of using Ultrasonic Nondestructive Testing of friction stir welds.

3.1.3.1. Visual Inspection

Perhaps the most straightforward inspection technique to use in FSW is the visual inspection. There is no need for special equipments and is truly an uncomplicated process. Visual inspection is an excellent means of inspecting the surface features of the weld material. It is very important because it may provide the probable location of the internal defect that may cause the breakage of the material. The limitation, obviously, is that it is only efficient on external inspection which is not appropriate for detecting root cracks of FSWs.

3.1.3.2. Liquid Penetrant Testing

Liquid penetrant testing is a method that reveals open discontinuities by bleed out of a liquid penetrant medium against a contrasting background developer. Kinchen and Aldahir performed an inspection of FSW aluminum alloy and discovered that penetrant testing is an unacceptable method due to poor detection and the excessive background noise produced by the surface, which interfered with the inspection. According to their study, due to the poor outcome, penetrant testing should include a removal of $(4 - 6) \times 10^{-4}$ inches of metal via caustic etch solution prior to the application of penetrant solution. But even though, this etching is applied, it didn't create a noticeable change in detection.

3.1.3.3. Magnetic Particle Testing

Magnetic particle testing is based on the principle that magnetic lines of force in a ferromagnetic material will be distorted by a distinct change in material continuity. If the discontinuity is open or close to the surface, the magnetic flux lines will be distorted at the surface, this they called flux leakage. The degree of

11

sensitivity of this method depends upon the size of the discontinuity. Sensitivity decreases with the decrease of the size of the crack and with the increase of the depth from surface of material. To be detected, the crack must be sufficiently large to interrupt magnetic field and cause external leakage. Micro cracks such as root to crack will not interrupt a magnetic field. In this case, magnetic testing is not advisable for inspection of root toe cracks in FSWs.

3.1.3.5. Radiography

Radiographic testing of weldments and brazements employs x-rays or gamma rays to penetrate an object and detect any discontinuities by the resulting image on a recording medium or viewing medium. Once the material is exposed to radiation, some of it will be absorbed and some will be scattered and transmitted to the metal. The level of absorption determines the contrast in the image output. Nonmetallic inclusions, pores, and aligned cracks result in more or less radiation that is why they are noticeable compare to the other parts. Kinchen and Aldahir test an FSW with the use of radiography. Test results demonstrated 90% probability / 95% confidence in this method's ability to detect cracks that are equal to or 30% of the material thickness. The problem arises with the inspection of dissimilar alloys. They found it not effective with dissimilar alloys due to some abrupt metallurgical change. As mentioned earlier, FSW is mostly used to combine dissimilar alloys, the reason why effectiveness of radiography is not enough for this study.

3.1.3.6. Eddy Current Testing

Eddy current testing is an electromagnetic nondestructive testing method in which eddy current flow is induced in the test piece. It is similar to magnetic testing aside from the fact that this one uses electrical energy. Changes in the flow of eddy currents caused by variations in the test piece are detected by a nearby coil and measured by suitable instruments. However, the results can be affected by variations in dimensions of the test piece and variation in physical and metallurgical properties of the test piece. With this kind of testing, reference standards are required.

12

The limitations and drawbacks of the mentioned nondestructive testing methods yield us to the utilization of ultrasound to do inspection in materials. The principal advantages of ultrasonic testing covers the limitations of the other methods. Some of these are:

1. It can detect discontinuities in thicker sections
2. It has relatively high sensitivity to small cracks
3. It is able to determine depth of internal inclusions and to estimate their size and shape
4. It can adequately inspect from one surface
5. it is no hazardous to personnel and other equipment

3.2. Ultrasonic Testing

Ultrasonic Testing (UT) uses high frequency sound energy to conduct examinations and make measurements. Ultrasonic inspection can be used for flaw detection or evaluation, dimensional measurements, material characterization, localization and sizing and more.

3.2.1. Basic Principles

Sound generated above human hearing (10 to 20 kHz) is called ultrasound. However, the typical frequency range employed in ultrasonic nondestructive testing is around 100 kHz to 50 MHz (Blitz, 1963). It behaves similarly as audible sound; the difference is that it contains much shorter wavelength. This means it can be reflected off small surfaces such as defects inside materials. Another thing is absorption coefficients are usually much higher and thus more easily measurable at higher frequencies.

13
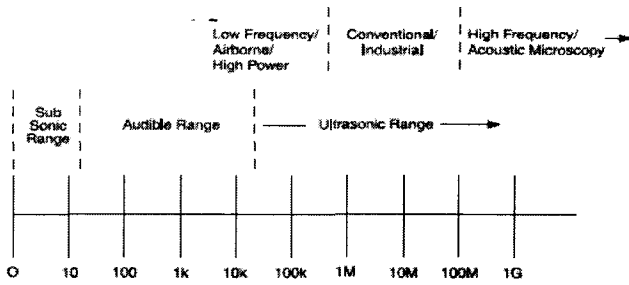
Figure 3.2.1-1 Ultrasonic Spectrum

(Figure from 'Fundamentals of Ultrasonics')

Advantages of ultrasonic testing comprise of detecting flaws in metallic and non-metallic materials, flaw's distances is possible to measure by just accessing from the material's surface, flaws can be detected in very thick materials, both internal and external flaws can be detected, flaw imaging is possible and material properties can be measured. This testing also contains a rapid speed and portable instrumentations. Equipment for automatic recording of inspection results is available and inspection costs are relatively low.

On the contrary, there are some shortcomings of ultrasonic testing. First is the difficulty in coupling energy to rough surfaces and impracticality to inspect complex shapes. It is also hard to detect and measure small tight crack when flaw imaging is complex rather than extensive. Training and experience are required for operators.
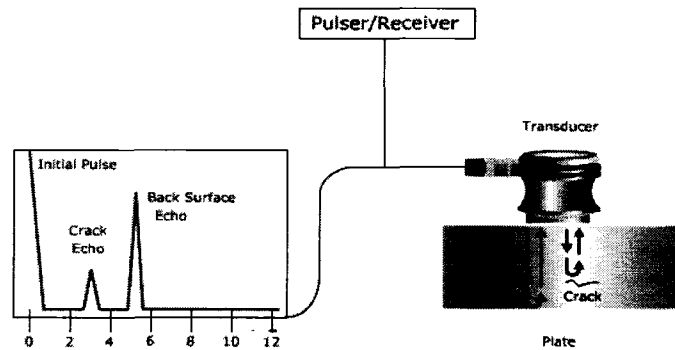
Figure 3.2.1-2 Typical ultrasonic testing inspection system.

(Figure from Ref. #8)

14

A typical UT inspection system is composed of the pulser/receiver, transducer and display devices (Ref. #8, Halmshaw, 1991 and McIntire, *et. al*, 1991). The pulser is an electronic device that produces high voltage electrical pulses. These pulses are applied to the transducer which has piezoelectric plates in it. These plates generate mechanical vibrations that are converted into sound energy. The sound energy is introduced and propagates through the materials in the form of waves. When there is a discontinuity, such as crack, in the wave path, part of the energy will be reflected back from the flaw surface. The reflected wave signal is transformed into an electrical signal by the transducer and is displayed on a screen. The time interval between the transmitted and reflected pulse is a measure of the distance of discontinuity from the surface of the materials and the size of the return pulse can be a measure of the size of the crack. From the signal, information about the reflector location, size, orientation and other features can sometimes be gained. In typical UT inspection system, the pulses are displayed in a scan on a time based on an oscilloscope screen. But recently, some systems were invented and they have their built-in display on it.

15
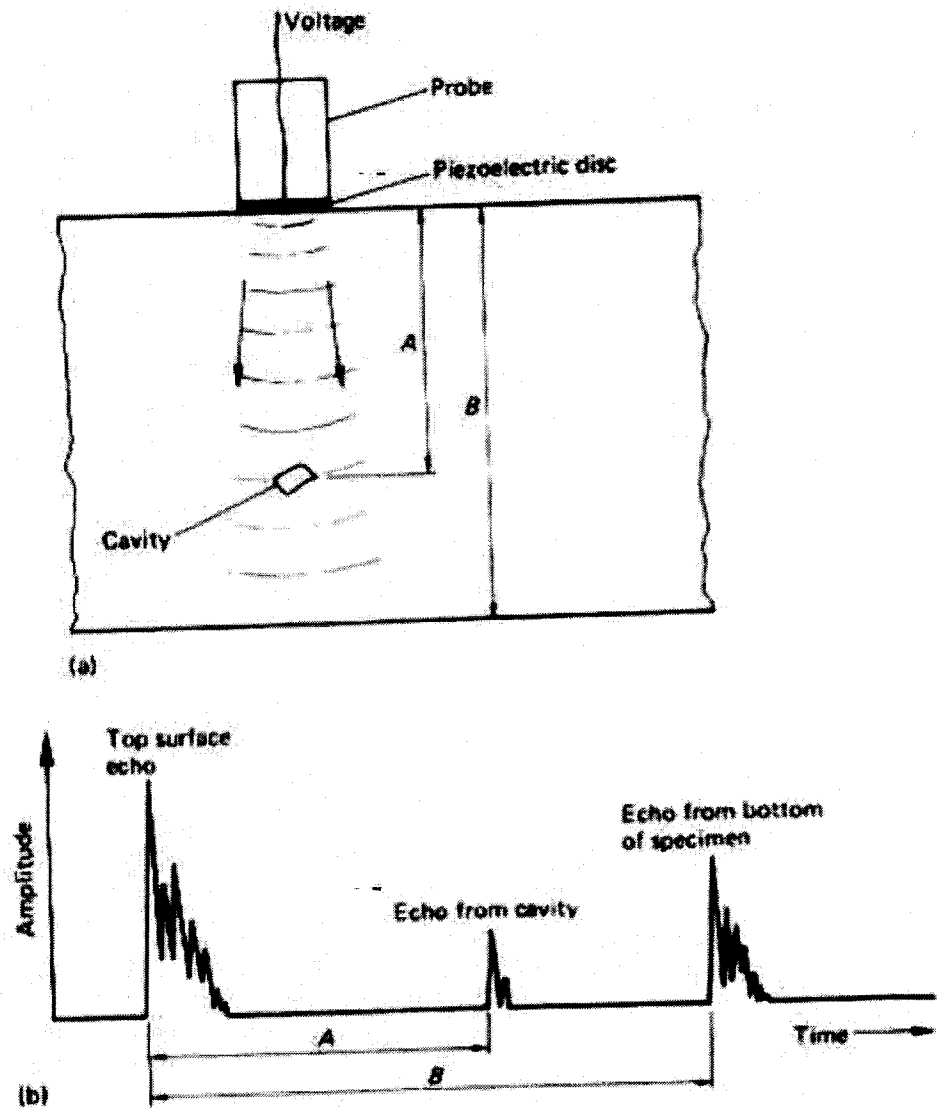
Figure 3.2.1-3 Contact Inspection and acquired A-scans from reflectors.
(Figure from "Nondestructive Testing" by Halmshaw)

3.2.2. Generation of Ultrasound

As mentioned, ultrasound energy travels in the material in the form of waves. Ultrasonic waves are mechanical vibrations, not electromagnetic radiation, and so have a different wavelength in different materials (Halmshaw, 1991). This is possible because of the elastic properties of the material and due to induced particle vibration in the material.

16

There are two main ways to irradiate ultrasonic waves. First is magnetostriction. This is usually used for underwater sounding and uses low frequency in the range of 100 kHz. Ultrasonic testing, however, needs higher frequency than this, and is therefore based on the second method of piezoelectricity. Piezoelectricity is a method of producing high-frequency oscillation. When an electric field is applied across the piezoelectric material, the polarized molecules will align themselves with the electric field, resulting in induced dipoles within the molecular or crystal structure of the material. This alignment of molecules will cause the material to change dimensions. This phenomenon is known as electrostriction. In addition, a permanently-polarized material such as quartz ($SiO2$) or barium titanate ($BaTiO3$) will produce an electric field when the material changes dimensions as a result of an imposed mechanical force. This phenomenon is known as the piezoelectricity.
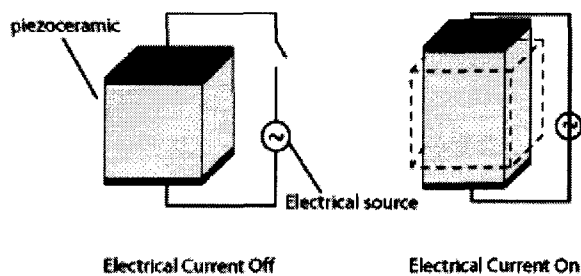
Figure 3.2.2 Illustration of piezoelectricity. *(Image from Ref. #11)*

3.2.3. Wave Modes

The mechanical vibration's movement determines the wave mode. In condense media, sound waves can propagate in four principle modes that are based on the way the particles oscillate. It can propagate as longitudinal waves, shear waves, surface waves, and waveguide waves. Longitudinal and shear waves are the two modes of propagation most widely used in ultrasonic testing. If the particle motion in a wave is along the line of the direction of travel of the wave, the resulting wave is called compressional wave or more known as *longitudinal wave*. On the other side, when the particle movement is at right angles with

17

respect to the direction of the wave, such waves are called transverse or *shear waves*. These usually contain a velocity which is half of the longitudinal velocity given the same material (Halmshaw, 1991). It is impractically incapable to transmit shear waves in liquids and gases so it can only attain appreciable distances only in solid bodies (Krautkramer, 1969).
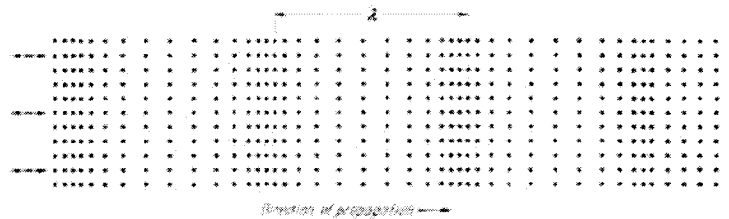
Figure 3.2.3-1 Illustration of longitudinal wave.
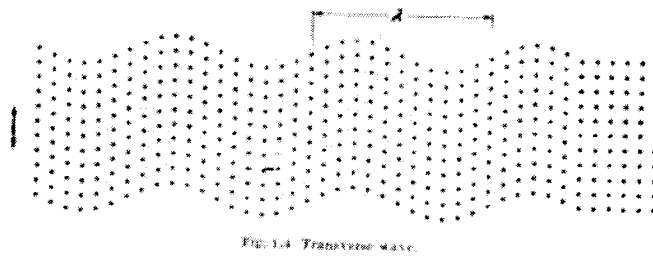
Figure 3.2.3-1 Illustration of shear wave.

(Both figures from "Nondestructive Testing" by Halmshaw)

Of course, ultrasound travels at different speed at different materials. As mentioned earlier, this is due the fact that the elastic properties of materials differ from one another. The velocities of the various kinds of ultrasonic wave can be calculated from the elastic constants of the material being inspected. For longitudinal waves, the formula for speed of sound is:

$$V_l = \left[\frac{E(1-\sigma)}{\rho(1+\sigma)(1-2\sigma)} \right]^{1/2}$$

While the shear wave velocity is given by:

18

$$V_s = \left[\frac{E}{2\rho(1+\sigma)}\right]^{1/2}$$

where E is the Young's modulus (Nm^{-2}), V_l is the longitudinal wave velocity, V_s is the shear wave velocity, ρ is the density of the material, and σ is the Poisson's ratio (Halmshaw, 1991).

3.2.4. Waves at Boundaries

Ultrasonic waves are reflected at boundaries where there is a difference in acoustic impedances of the materials on each side of the boundary. This is commonly known as impedance mismatch. The greater the impedance mismatch, the greater the percentage of energy that will be reflected at the interface or boundary between one medium and another (David and Cheek, 2002).

Case 1: Normal Incidence

Consider here a simple case of a plane wave striking a smooth simple boundary at right angle.

incident

reflected

Medium 1

Medium 2

transmitted
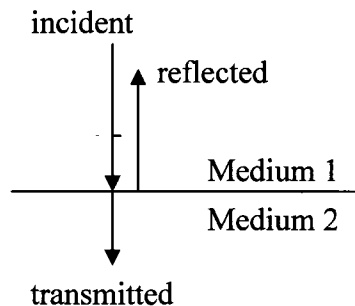
Acoustic impedance is important in determining the transmission and reflection coefficient between two materials which can be computed as follows:

$$T = \frac{4Z_1 Z_2}{(Z_1 + Z_2)^2}$$

19

$$R = \left(\frac{Z_1 - Z_2}{Z_1 + Z_2}\right)^2$$

These formulae are valid for both longitudinal and shear waves, but as shear wave can't travel in liquid, it is always completely reflected at a solid/liquid or solid/gas interface.

Case 2: Oblique Incidence

If a sound wave strikes a plane interface obliquely, at a certain angle of incidence with respect to normal, reflected and transmitted waves arises as in optics.
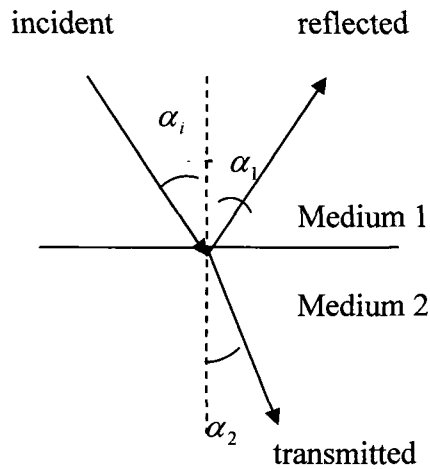
The reflection and transmission coefficients are solved by:

$$R = \frac{\dfrac{Z_2}{\cos\alpha_2} - \dfrac{Z_1}{\cos\alpha_1}}{\dfrac{Z_2}{\cos\alpha_2} + \dfrac{Z_1}{\cos\alpha_1}}$$

$$T = \frac{2\dfrac{Z_2}{\cos\alpha_2}}{\dfrac{Z_2}{\cos\alpha_2} + \dfrac{Z_1}{\cos\alpha_1}}$$

20

And with this case, Snell's Law is formed. This relationship is shown in this equation:

$$\frac{\sin \alpha_1}{\sin \alpha_2} = \frac{V_1}{V_2}$$

- -

- -

- - 21

CHAPTER IV

ULTRASONIC TESTING OF FRICTION STIR WELDS

4.1. Optimization of Several Ultrasonic Techniques

Recalling, it was stated in Chapter 1 of this thesis that the major problems that was encountered in investigating FSW with conventional ultrasonic testing; specifically normal beam pulse echo technique. The reasons are mainly because of the unique characteristics of FSW process and the limitations of normal beam inspection in these kinds of investigation, as stated on the said chapter. In this chapter, the method used is to analyze the sensitivity of several ultrasonic technologies and aimed to determine which one will provide the best detection capability.

4.1.1. Scanning Acoustic Microscopy

Scanning Acoustic Microscopy is a viable nondestructive method that has a high-resolution defect visualization to determine elastic parameters in both the medical and industrial fields (Tittman and Miyasaka and Ohno, 1988). In using SAM, the sound beam is focused; up to sub micrometer size, and has a high frequency, 10MHz to 3GHz. The resolution of the system is comparable to an optical microscope. In addition to image formation, the SAM can detect the amplitude and the phase of a reflected wave so by analyzing them, the elastic properties may be quantitatively determined. The SAM may operate in two modes: first is called tone-burst-wave mode and the other one is pulse-wave mode. Both modes provide an adequate resolution but pulse-wave mode has better penetration competence. It can penetrate to up to 1 cm by using 10 to 100 MHz transducer's frequency. Hence, in our case, the pulse-wave mode was used to observe deep interior of our FSW sample where the root crack is located.

22

The image below is the schematic diagram of a scanning acoustic microscope. The imaging mechanism of a SAM with water as couplant is described.
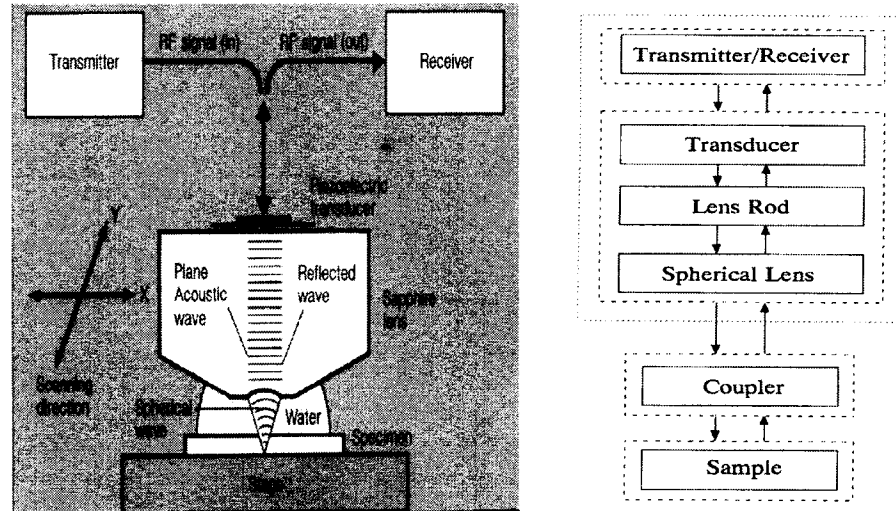
Figure 4.1.1-1 Imaging mechanism of SAM. *(Figure from "Scanning Acoustic Microscopy")*

An electrical signal is generated by a source or a pulser that gives a spike pulse wave or only a few cycles. This electrical signal is transmitted to a piezoelectric transducer located on the top of a buffer rod. The electrical signal is then converted to an acoustic signal by the transducer. Refer to Chapter 3 for explanation on how transducer works. The buffer rod serves as a delay line to separate the initial pulses from the reflections from the specimen. Most buffer rods are made of fused quartz, sapphire or those materials that have high velocity compared to that of a coupling medium and having low attenuation. The diameter of the rod is determined to be larger than the diameter of the transducer and the length should be longer than the near-field region which is calculated by:

$$N = \frac{D^2}{4\lambda}$$

wherein N is the near-field region, D is the diameter of the transducer and λ is the wavelength of the material used for the buffer rod.

The acoustical signal that comes out of the transducer is a plane wave. This plane wave becomes spherical wave as it travels through the buffer rod and reaches the lens' bottom. The lens' bottom geometry is designed to focus the

23

ultrasonic beam. The paraxial focal distance of the acoustic lens is approximately expressed as

$$F_0 = \frac{R}{(1 - C')}$$

$$C' = \frac{C_2}{C_1}$$

where R is the radius of the curvature of the surface of the lens, C_1 is the longitudinal wave velocity of the buffer rod, and C_2 is the longitudinal wave velocity of the coupling medium.

The radius of curvature of the lens is determined by considering the operating frequency and attenuation coefficient. The table below shows the range of radii corresponding to various frequencies.

Table 4.1.1-1 Frequency and corresponding radius

Frequency	Radius
100 MHz	1 – 2 mm
200 MHz	500 μm – 1 mm
400 MHz	500 μm
800 – 1000 MHz	125 μm
1.5 – 3 GHz	50 μm

The aperture angle of the lens is determined by the focal distance. When the focal distance and the aperture angle are known, the radius of the aperture is determined by

$$r = F_0 \sin\left(\frac{\theta_\alpha}{2}\right)$$

where r is the radius of aperture, F_0 is the focal distance and θ_α is the aperture angle.

24

The ultrasonic beam created is then focused within the specimen and reflected from the specimen. The reflected ultrasonic beam now carrying the acoustic information of the specimen is again converted into plane wave by the lens. The plane wave returns to the transducer through the buffer rod. This plane wave is converted back to electrical signal at the transducer. The electrical signal maybe amplified to provide an interpretable signal on the monitor connected to the system.

Suppose that a pulse wave emitted from the acoustic lens through the coupling medium is focused onto the back surface of the specimen, and suppose that the pulse wave is strong enough to travel through the specimen and reflect back to the acoustic lens. If the material is layered, the timing of each reflection is different because the travel distance is different. See figure 4.1.1-2.
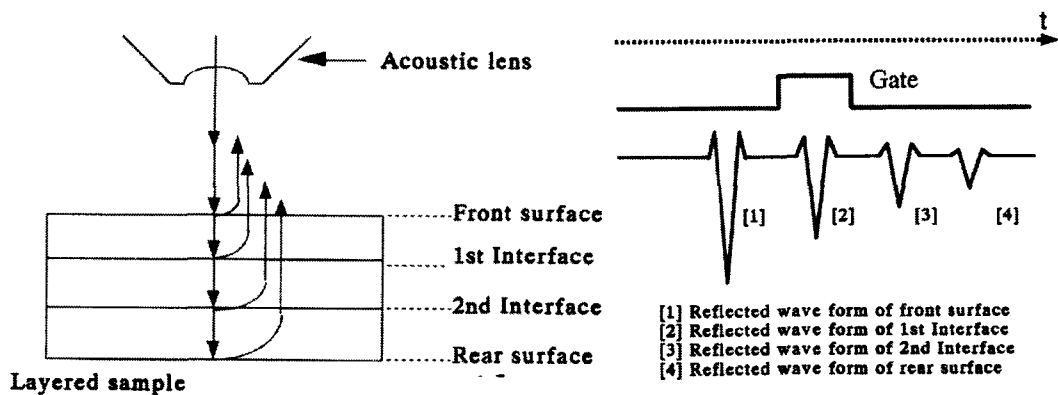
Figure 4.1.1-2 SAM focused on different layer and gating process.
(Figures from "Scanning Acoustic Microscopy")

The display shows the reflected signal that has pulses from different surfaces of the material. The pulse wave can be focused wherever in the material, according to the interest. This flow of processes allows information that is collected at a single spot on a specimen. To form an acoustical image, 2-dimensional or 3-dimensional, there should be a raster scanning on the material. The lens is mechanically scanned in the x and y direction of the material to form an image frame which is usually called a B-scan or a C-scan in ultrasound images.

25

4.1.2. Angled Beam Inspection

Although a greater part of ultrasonic testing is done with longitudinal waves propagating normal to the test object's surfaces, there are also instances when an angled beam is preferred. The predominant reason for angle beam testing is the detection of discontinuities or cracks with geometries and orientations other than parallel to the test surface (Krautkramer, 1969 and McIntire, 1991). Some examples of these defects are planar cracks normal to the test object's surface, voids with small reflective surfaces and discontinuities in welds with uneven top surface such as FSW.

When an ultrasonic wave is propagating in a homogeneous medium passes through an interface at a normal incident angle where the velocity of the second medium is different, the incident wave is reflected and transmitted with out any change in propagation direction. However, when an ultrasonic wave propagating in a homogeneous medium passes through any angle but 90° the incident wave is mode converted and refracted. These phenomena may affect the entire beam or only a portion of the beam and the sum total of the changes that occur at the interface depend on the angle of incidence and the velocity of the ultrasonic waves leaving the point of impingement on the interface. Figure 4.1.2-1 shows the relationship of possible reflected and refracted waves of an incident longitudinal wave in a liquid and solid interface (Ref. # 7-12).
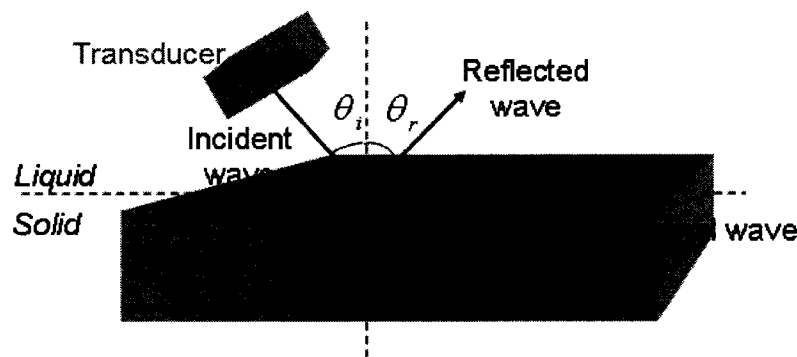
Figure 4.1.2-1 Angled beam testing principle.

26

The reflection and refraction of these ultrasonic waves are governed by the acoustic analog of Snell's Law:

$$\frac{\sin \theta_i}{v_i} = \frac{\sin \theta_l}{v_l} = \frac{\sin \theta_s}{v_s} = \frac{\sin \theta_{sf}}{v_{sf}}$$

where $\sin \theta_i$, $\sin \theta_l$, $\sin \theta_s$ and $\sin \theta_{sf}$ are the ray propagation angles with respect to normal and v_i, v_l, v_s and v_{sf} are the velocities of the incident longitudinal wave, longitudinal, shear and surface wave in the material.

Referring to the Figure 4.1.2-1, if the angle of incidence is small, the incident wave undergoes a mode conversion at the interface, resulting in the simultaneous propagation of longitudinal and shear wave in solid. If angle of incidence is increased, the direction of refracted longitudinal wave will approach the plane of the liquid-solid interface; $\theta_l \to 90°$. At the first critical angle, $\theta_l = 90°$ the refracted longitudinal wave will disappear, leaving only a refracted mode converted shear wave to propagate in the solid. If angle of incidence is increased beyond the first critical angle, the direction of the refracted shear wave will approach the plane of the interface, $\theta_s \to 90°$. At this second critical angle, $\theta_s = 90°$, the refracted shear wave will disappear and the incident wave is only reflected at an angle equal to the incident angle and there will be an appearance of a surface wave.

4.1.2.1 Single Element

In angle beam testing with the beam directed away from the transducer, no back surface reflection is present on the monitor display. The appearance of reflected signal usually signifies the presence of a discontinuity.

27
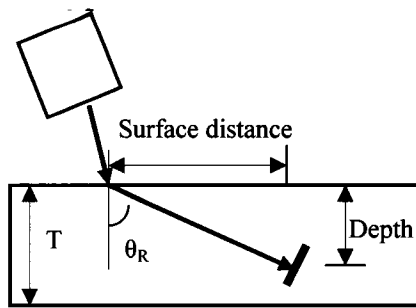
Figure 4.1.2.1-1 Single element angled beam inspection.

Consider the image above; the ultrasound propagates in the refracted shear wave direction and once it hits any discontinuity, it will give a reflected signal back to the transducer. In this case, the location and depth of the crack maybe be determined as long as the velocity of ultrasound and the time of flight are known in priori.
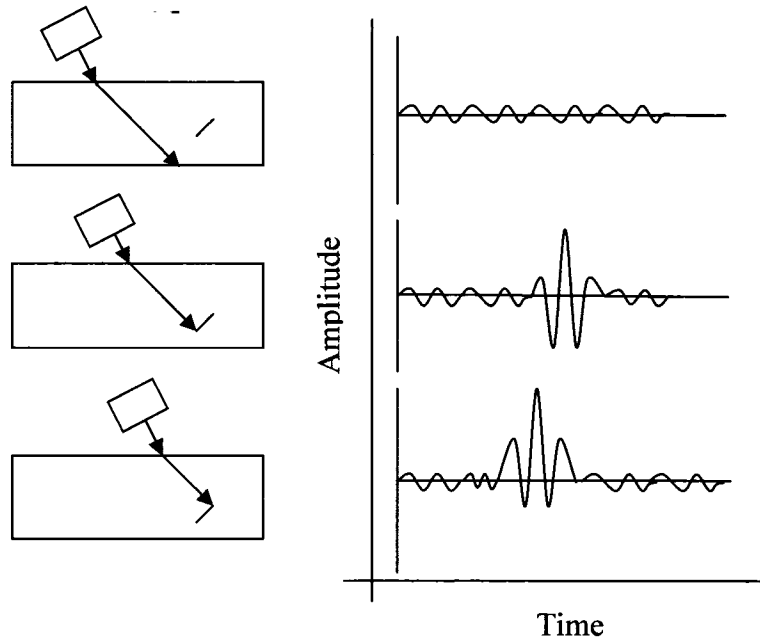
Figure 4.1.2.1-2 Localization and sizing.

28

The location of the crack is calculated by:

$$sd = path \times \sin \theta_s$$
$$depth = path \times \cos \theta_s$$
$$path = \frac{t \times v_s}{2}$$
$$length = (t_1 - t_2) \times v_s / 2$$

wherein sd is the surface distance, $depth$ is the depth of the crack from the surface, $path$ is the distance the ultrasound travels inside the material, t is the time of flight, t_1 is from the bottom of the crack, t_2 is from the tip of the crack, v_s is the shear wave velocity and $length$ is the size of the crack.

4.1.2.2 Phased Array Technology

Most conventional ultrasonic inspections use monocrystal probes with divergent beams. The ultrasonic field propagates along an acoustic axis with a single refracted angle. The divergence of this beam is the only additional angle, which might contribute to detection and sizing of misoriented small cracks. This is improved with Phased Array Technology.

Imagine a monoblock is cut in many identical elements, each with a width much smaller than its length. Each small crystal may be considered a line source of cylindrical waves. The wave fronts of the new acoustic block will interfere, generating an overall wave front. The phenomenon of phased array probes follows the Huygens Principle (Moles *et. al*, 2004). The small wave fronts can be time-delayed and synchronized for phase and amplitude, in such a way as to create an ultrasonic focused beam with steering capability.

The main feature of phased array ultrasonic technology is the computer controlled excitation of individual elements in a multi element probe. The excitation of piezocomposite elements can generate an ultrasonic focused beam with the possibility of modifying the beam

29

parameters such as angle, focal distance and focal spot size through software. The sweeping beam is focused and can detect in specular mode the misoriented cracks. These cracks maybe located randomly away from the beam axis. A single crystal probe, with limited movement and beam angle, has a high probability of missing misoriented cracks and cracks located away from the beam axis.
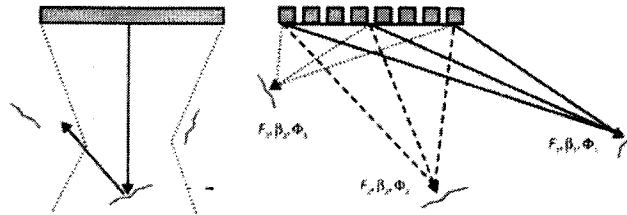
Figure 4.1.2.2-1 Comparison of single element and phased array probes.
(Figures from R/D Tech Book)

To generate a beam in phase and with a constructive interference, the various active probe elements are pulsed at slightly different times. During transmission, the acquisition instrument sends a trigger signal to the phased array instrument. The latter converts the signal into a high-voltage pulse with a preprogrammed width and time delay defined in the focal laws. Each element receives one pulse only. This creates a beam with a specific angle and focused at a specific depth. The beam hits the defect and bounces back. The signals are received, then time-shifted according to the receiving focal law. They are then reunited together to form a single ultrasonic pulse that is sent to the acquisition instrument.
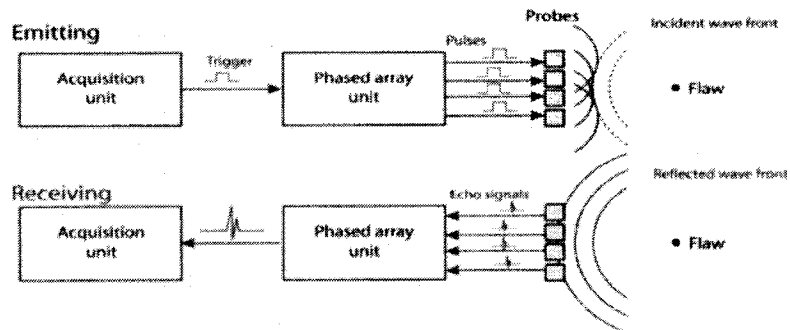
Figure 4.1.2.2-2 Beam creation.
(Figure from R/D Tech Book)

30

Beam steering is the ability to dynamically synthesize an ultrasonic beam of any angle within the overall beam spread of an individual element by sequentially firing each element in an array to create a wave front following a desired angle. Selecting the array firing order and pulse delays can also be used to dynamically focus an ultrasonic beam. Both beam steering and dynamic focusing can be changed on a pulse by pulse basis to effectively sweep through test material. They may also be combined to give a resultant beam both focused and angled.
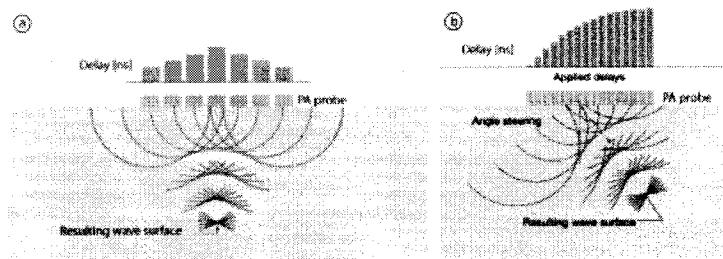
Figure 4.1.2.2-3 Beam Steering and Beam Focusing.
(Image from R/D Tech Book)

Based upon geometry and arrangement of the transducer elements, the array probes are divided into three types: annular arrays, linear arrays and planar arrays. Diagrams are shown below.
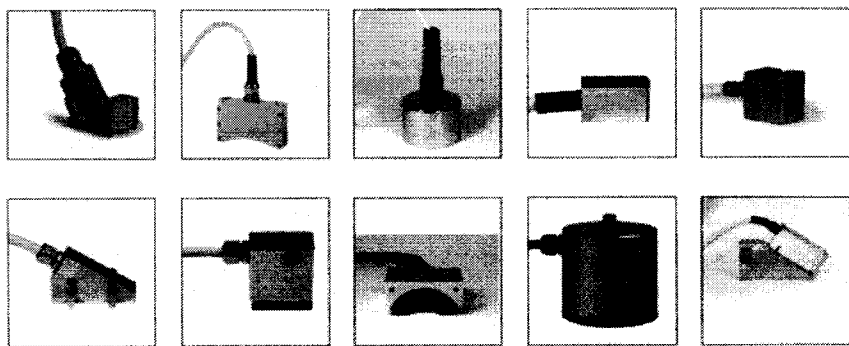
Figure 4.1.2.2-4 Different types of ultrasonic phased array probes.
(Image from R/D Tech Book)

Annular arrays are-composed of concentric arranged rings and by properly applying time delays on it, sound beam can be focused to

31

different depths of the specimen or can produce a long and narrow focus tube. It has the advantage that the pressure distribution is symmetrical with respect to the beam axis; however, variation of incidence angle is not possible. Linear arrays are the ones that are mostly used today. They are divided into bars that have a width that varies between one and one-half of the ultrasonic wavelength. The ultrasonic field pattern can be influenced only in one plane, again by applying proper delay. In these types, beam steering and focusing is possible and the side-lobe level can be reduced by optimizing the probe parameters. The excitation of longitudinal and shear wave is also possible. Lastly, in planar arrays, the transducer elements are distributed two-dimensionally. Only with this array type is three-dimensional beam forming is possible (Gebhardt, 1983). Due to the fact that linear array can do beam steering and focusing and can provide ultrasonic shear wave in the material, it was utilized in this thesis and the study of the inspection improvement will be based on its characteristics and properties.

Annular Phased Array Probe

Linear Phased Array Probe

2D Matrix Phased Array Probe
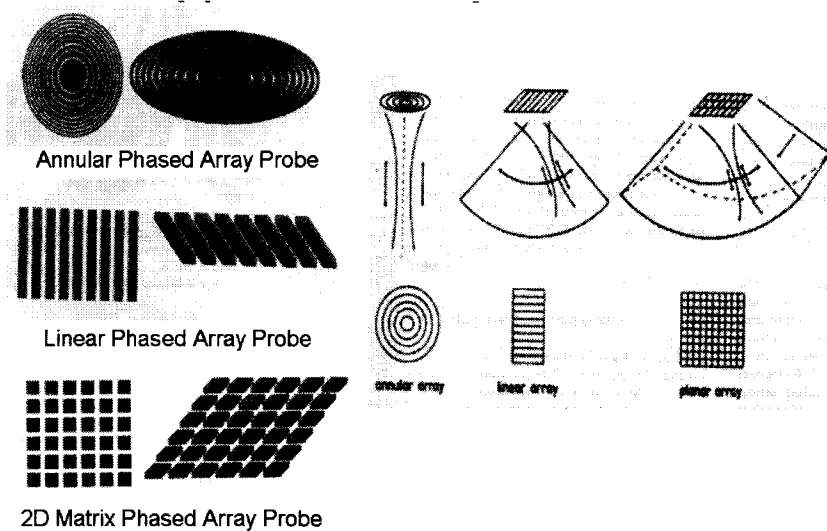
Figure 4.1.2.2-5 Annular array, linear array and matrix array.

(Figures from R/D Tech book and "Improvement of Ultrasonic Testing")

There are a lot of ways on how ultrasonic testing is improved by utilizing phased array technology. First of all is the improvement in

32

moving the transducer itself. There is no need for mechanical scanning. It also improves reliability of detection by providing higher signal to noise ratio and it progresses accessibility factors. These advantages will be profoundly converse on the next few paragraphs.

4.1.2.3 Improvements of Phased Array over Single Element

Pressure distribution and beam directivity and even reduction of side-lobes have been mentioned sometime in this thesis. These things will be the basis of how phased array inspection was improved compare to single element testing.

Beam directivity is dramatically improved with phased array probe. How, by having more number of elements, by increasing its inter-element spacing and by decreasing the steering angle. Why by these parameters beam directivity is improved? The explanations below answer this question.

The linear phased array was modeled as a discrete number of simple sources separated by equal distances between the elements.
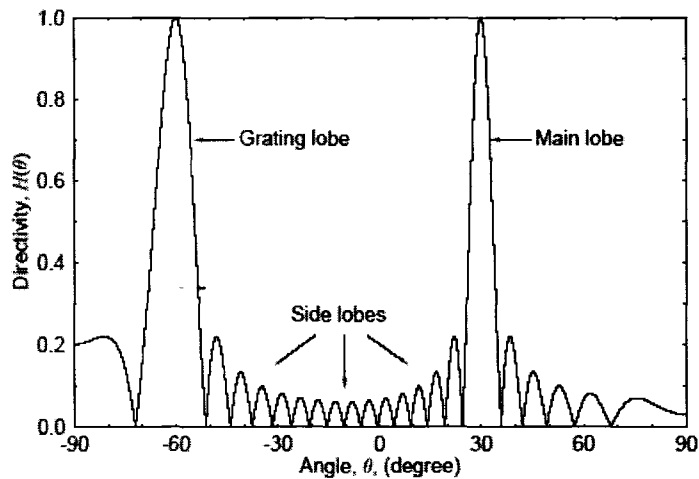
Figure 4.1.2.3-1 Acoustic pressure distribution.

The pressure field was constructed using Huyghens' principle with properly selected phases and amplitudes as follows:

33

inspection speed. With phased array probes, inspection becomes more flexible. Different angles and different depths can be inspected without

$$p(r,\theta,t) = \frac{p_0 r_0}{r} \frac{\sin\left[\left(\dfrac{\omega\Delta\tau - kd\sin\theta}{2}\right)N\right]}{\sin\left(\dfrac{\omega\Delta\tau - kd\sin\theta}{2}\right)} \exp\left[-j\left(\frac{\omega\Delta\tau - kd\sin\theta}{2}\right)(N-1)\right] \times \exp[j(\omega t - kr)]$$

for $r>>d$, where r_0 is the infinitesimally small radius of pulsating point sources, p_0 is the pressure amplitude at the simple point source, k is the wave number, w is the angular frequency, N the number of point sources, and j is a unit imaginary number (Wooh and Shi, 1998). The required time delay between the adjacent sources to steer the beam at an angle θ_s is given by the relationship

$$\Delta\tau = \frac{d\sin\theta_s}{c}$$

where c is the wavespeed in the medium.

The beam directivity is analyzed this time in order to understand the steering characteristics quantitatively. The directivity, $H(\theta)$ defined as the pressure at an angle normalized by the pressure at the steering angle, can be written from the long equation above in the form of

$$H(\theta) = \left[\frac{\sin\left[\pi d\left(\dfrac{\sin\theta_s - \sin\theta}{\lambda}\right)N\right]}{N\sin\left[\dfrac{\pi d(\sin\theta_s - \sin\theta)}{\lambda}\right]}\right]$$

where the variables stand for the same values as in the definition of pressure field mentioned earlier.

With these mathematical expressions of beam directivity and by properly selecting transducer parameters that influences the wave propagation characteristics; phased array can be optimally designed to increase detection capability. The figure below is a schematic illustration that shows some important features of directivity plots; the main lobe, side lobes and grating lobes. The main lobes appear exactly in the steering direction, while the side lobes appear in many directions other than the steering angle. In addition, there exists the grating lobe whose magnitude is exactly equal to the main lobe but appears at the *(N-1)th* lobe location from the main lobe. The steering performance can be characterized by the

34

sharpness of the main lobe and the amount of side-leaking energy. Therefore, by determining optimum transducer design, sharpest main lobe and suppressed side lobes and squelched grating lobes are required (Wooh and Shi, 1998 and Moles *et. al,* 2004).

The beam directivity at a certain steering angle can be quantified by the width of the lobe in that direction that is defined by the zero-crossing points of the lobe. The main lobe sharpness factor is a quantitative representation of the beam directivity in the steering direction. From equation above, that main lobe sharpness factor is derived as

$$q = \frac{1}{\pi}\left[\sin^{-1}\left(\sin\theta_s + \frac{\lambda}{Nd}\right) - \sin^{-1}(\sin\theta_s - \frac{\lambda}{Nd})\right]$$

Smaller q means that the lobe is sharp and the beam is finely directed. And this q has the parameters of a phased array probe so by aiming to have a smaller q, this parameters should be designed properly. When the number of elements N approaches an infinitely large number, the q approaches zero (Wooh and Shi, 1998). This is an ideal condition but is impossible to achieve because of limitations of control electronics. And of course, by increasing number of elements, transducer dimension also increases which is not ideal because transducer will be bulkier and heavier and it will not be accessible in that manner. Therefore it is necessary to find a reasonably low number of elements that does not detrimentally affect these practical considerations.

Figure 4.1.2.3-2 Main lobe sharpness factor vs. # of elements & steering angle.
(Figures from "Optimization of Ultrasonic Phased Arrays")

35

It is also straightforward to show that q is an increasing function with the steering angle. Given an example below, lobe sharpness increases and the directivity degrades with an increasing steering angle. The degradation rate is slow at first but accelerates rapidly as the steering angle reaches certain value, like 60° in this case.

Also, another way to reduce main lobe factor is by providing a larger inter-element spacing for a fixed λ. Figure below shows directivities in polar form, showing the effect of d on the beam directivity. By comparing the lobe widths, one can observe that the beam directivity in the steering direction is greatly improved by increasing inter-element spacing. However, if it is too high, there are more side lobes and grating lobes produced. So to solve this problem, one should know the critical inter-element spacing that introduces the first grating lobe, providing the best directivity, yet squelching the grating lobes. This critical condition can be found from H equation for

$$H(-\pi/2) = 1$$

For example, the inter-element spacing that satisfies the condition

$$\sin\theta = \sin\theta_s - \frac{\lambda}{d}$$

at $\theta = -90°$ is the critical inter-element spacing d_{crv}. In other words,

$$d_{CR} = \frac{\lambda}{1 + \sin\theta_s}$$

where θ_s is the maximum desired steering angle.

36
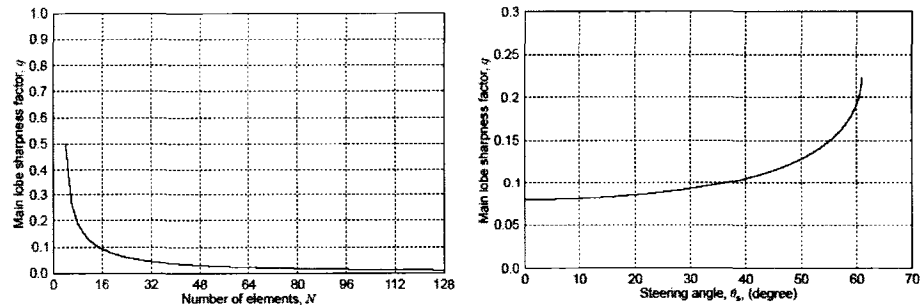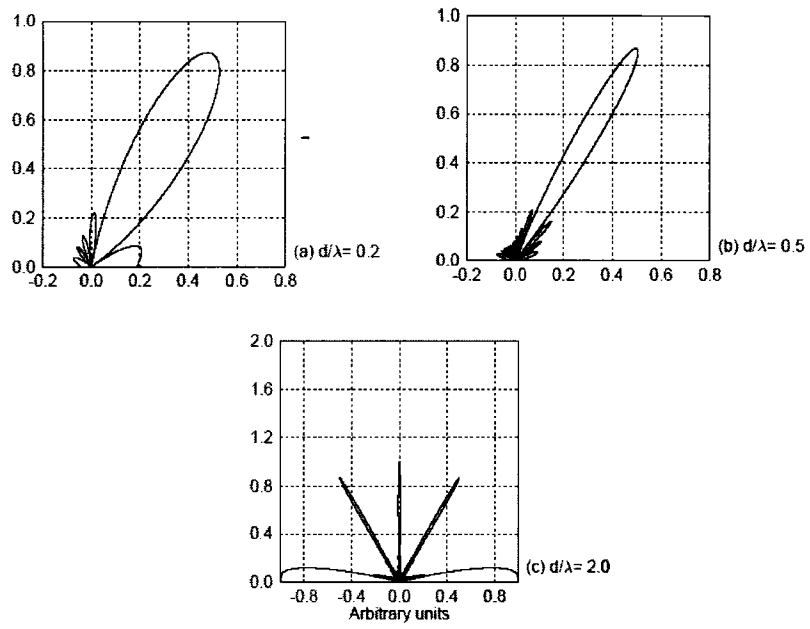
Figure 4.1.2.3-3 Main lobe sharpness factor vs. element spacing.

(Figures from "Optimization of Ultrasonic Phased Arrays")

37

4.2. FSW Inspection with Different Techniques

4.2.1. Description of Specimens
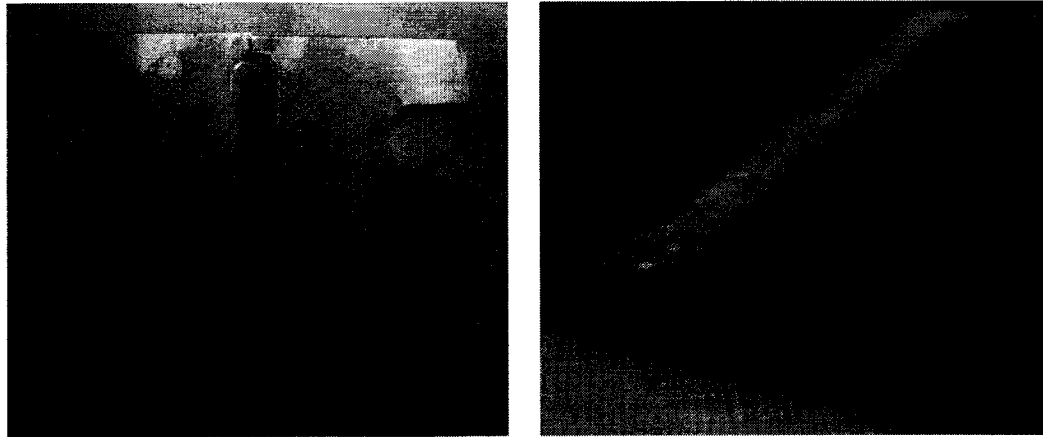
Figure 4.2.1-1 Friction Stir Weld Sample.
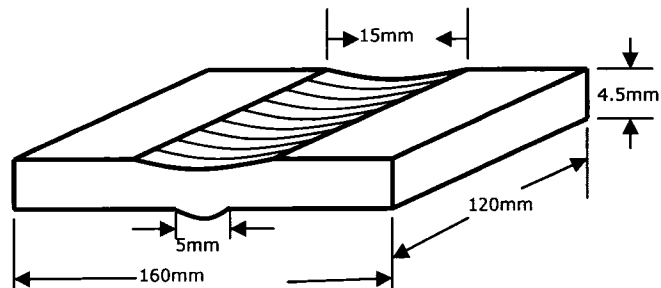
Figure 4.2.1-2 FSW sample dimensions.

The real FSW samples are made up of aluminum sheets welded side by side. There are six preliminary samples that vary their thicknesses from 4.35 cm to 4.85 cm. Samples are shown on Figure 4.2.1-1. They have a very rough top surface which was created due to FSW process. Its width is about 15mm wide. The center line of the weld at the bottom has a curve like shape that may have a width of about 5mm and height of 1mm. Second batch of samples were investigated but this samples are a little thinner than the previous ones. And one more observation was that instead of having a curve like bottom shape, these ones contain a rectangular step at the weld line at the bottom surface. The steps have a

38

height of approximately 1mm as well. These samples have been previously inspected using a destructive technique. See Figure 4.2.1-3.
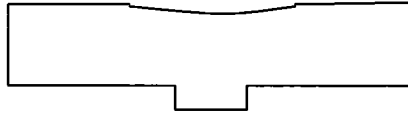
Figure 4.2.1-3 Profile of second batch of FSW samples.
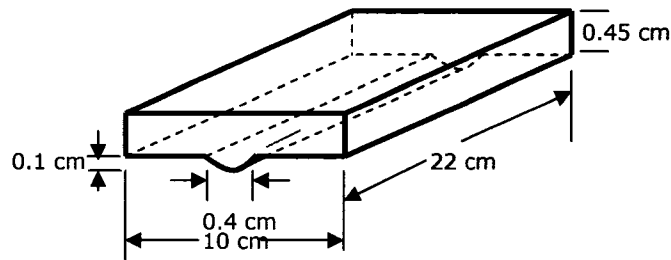
Figure 4.2.1-4 Synthetic FSW sample.

Due to the fact that at the preliminary experiments bestowed an un-interpretable responses in A-scans, synthetic sample was needed to basically understand signal behavior of sample with uneven surfaces and curve like bottoms. These samples are also made up of aluminum sheets but not welded. It has smooth flat top surface and it doesn't have any metallurgical changes. It also has a curve like bottom with 1mm depth and approximately 4mm width. This is to make a replica of the shape of the real FSW sample. It has 45 mm thickness and it is 22cm long and 10cm wide. In some known locations, a flaw was formed. The purpose was to compare ultrasound responses from those portions that are clean and those portions with known flaw details. The flaw was done by marking a line with a paper cutter along the supposed to be weld line that has a depth of approximately 50µm and higher.

39

4.2.2. Inspection Procedures

4.2.2.1 Sonix Scanning Acoustic Microscopy

The specimen (real FSW and synthetic) was immersed into a container filled with distilled water at a room temperature. The acoustic lens used has a frequency of 25 MHz and was also immersed into the water. The water serves as the coupling medium because sound waves can not travel in vacuum. The lens was focused at the bottom surface of the curve like/rectangular shape of the specimen. This was done to view the overall internal structure of the welded sample. B-scans were taken to analyze images and signals if they might indicate some sort of cracks present in the root of the weld specimen.

Surface reflection   Bottom reflection
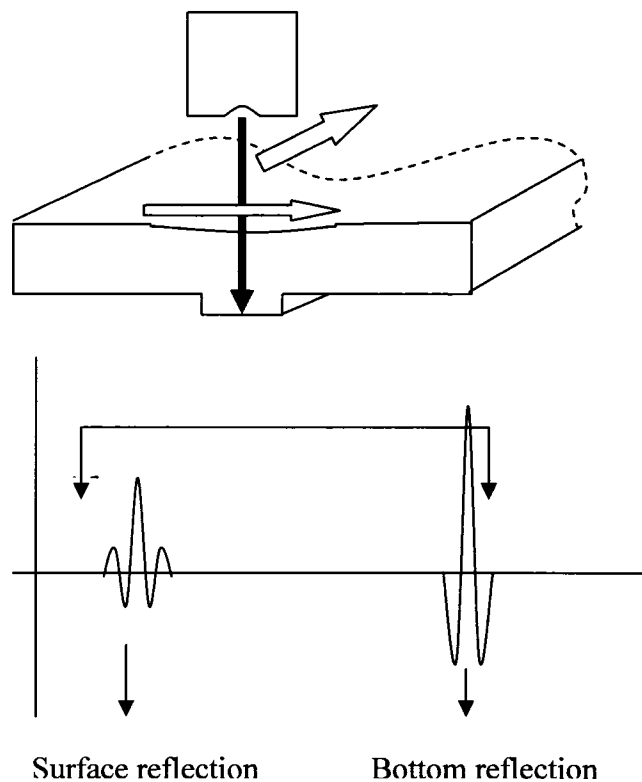
Figure 4.2.2.1-1 SAM inspection and gating.

40
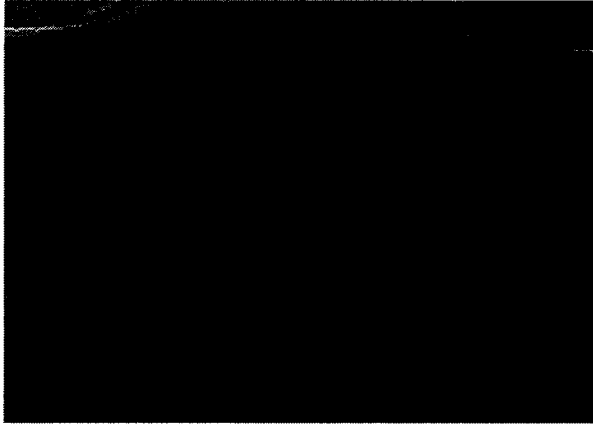
Figure 4.2.2.1-2 B-scan of Aluminum FSW with 4mm thickness.

The ultrasound beam is known to be focused at the bottom if the reflection pulse from the bottom is at its maximum value; amplitude is at the maximum value. The gate was put from the beginning of the surface reflection up to the end of the bottom response. See Figures 4.2.2.1-1 and -2. In this case all information between surface response and bottom response will be shown on a B-scan image. The samples were scanned from end to end and multiple B-scans were recorded. This was equivalent to viewing the internal structure of the welded line of the specimen by having the z- direction focused at the bottom and having raster scan in x- and y- direction.

4.2.2.2 Angled Beam Single Transducer

Using a single element immersion transducer, V2098 with 15MHz and 0.157" diameter, the synthetic samples and real FSWs were inspected in the same part of interest. The incident angles used was $20°$ and $23°$ with respect to normal to create a $45°$ and $60°$ refracted shear wave onto the metal samples. Shear wave was used to lessen mode conversion. These angles were computed as follows, knowing the speed of sound in water and in aluminum:

$$\theta_i = \sin^{-1}\left[\left(\frac{\sin 45°}{3200m/s}\right) \times 1500m/s\right]$$

41

wherein 3200 m/s is the shear wave velocity in aluminum and 1500 m/s is the longitudinal wave speed in water.

The transducer was also focused to the bottom surface. In this case the ultrasound waves are in form of plane waves unlike in the SAM wherein the lens used utilizes spherical waves. This inspection is done manually and A-scans were observed and recorded.
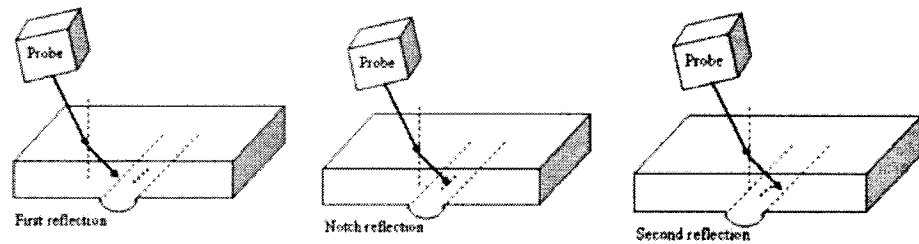
Figure 4.2.2.2-1 Single element angled beam inspection with synthetic samples.

For example, the image above illustrates the scanning done with the synthesized samples; the portion where the notch is located. Since angled beam inspection eliminates the response from the top surface, reflection were interpreted as reflection from the bottom reflectors such as the first step, the notch and the second step. Example A-scans are shown below, A-scans with notch-and A-scans without.
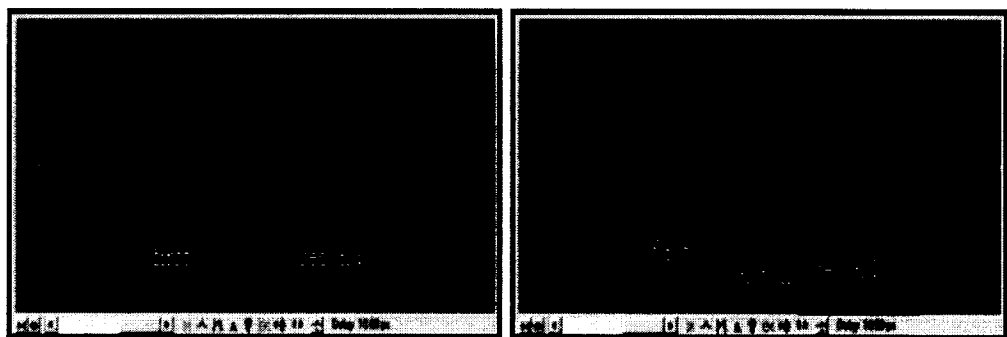
Figure 4.2.2.2-2 A-scans of synthetic sample in the portion with notch and without.

42

4.2.2.3 Angled Beam Phased Array

Basically, the method of angled beam inspection using phased array is the same as the methods with single element. The only difference is the transducer used and the monitor or acquiring system used. Instead of using a single element transducer, the transducers used were a 32 element R/D array transducer with 10MHz frequency and 0.31mm pitch size and a 52 element matrix array with 15MHz frequency and 1.25mm pitch size. One more device was used, R/D Tech Omniscan, which is specialized for phased array scans. Sectorial scans were recorded from this device.

43

4.3. Results and Discussions

4.3.1. Results from SAM

It has been mentioned for few times in this thesis that normal beam inspection has some limitations in detecting root cracks because of the crack's nature and ultrasound's capability; the main reason why Sonix Microscopy provided some limited but significant results. The B-scan images show the profile of the FSW and in some ways shows some significant portion of the material and some defects such as delamination which is parallel to the inspection surface. With the B-scans of the synthesized sample, there is somewhat an obvious difference in the portion with notch and without notch even if it is very small and tight. This proves the sensitivity of ultrasound to detect micro cracks.

The illustration of the scanning procedure and the C-scan and B-scan images from the samples using 25MHz acoustical lens are shown on Figure 4.3.1-1. The focus is at the bottom of the weld line to view the whole internal of the weld sample. B-scans were gated to view the curved part of the weld line at the bottom of the sample. 50 frames of B-scan images were acquired to observe some significant difference in the image that might determine a crack.
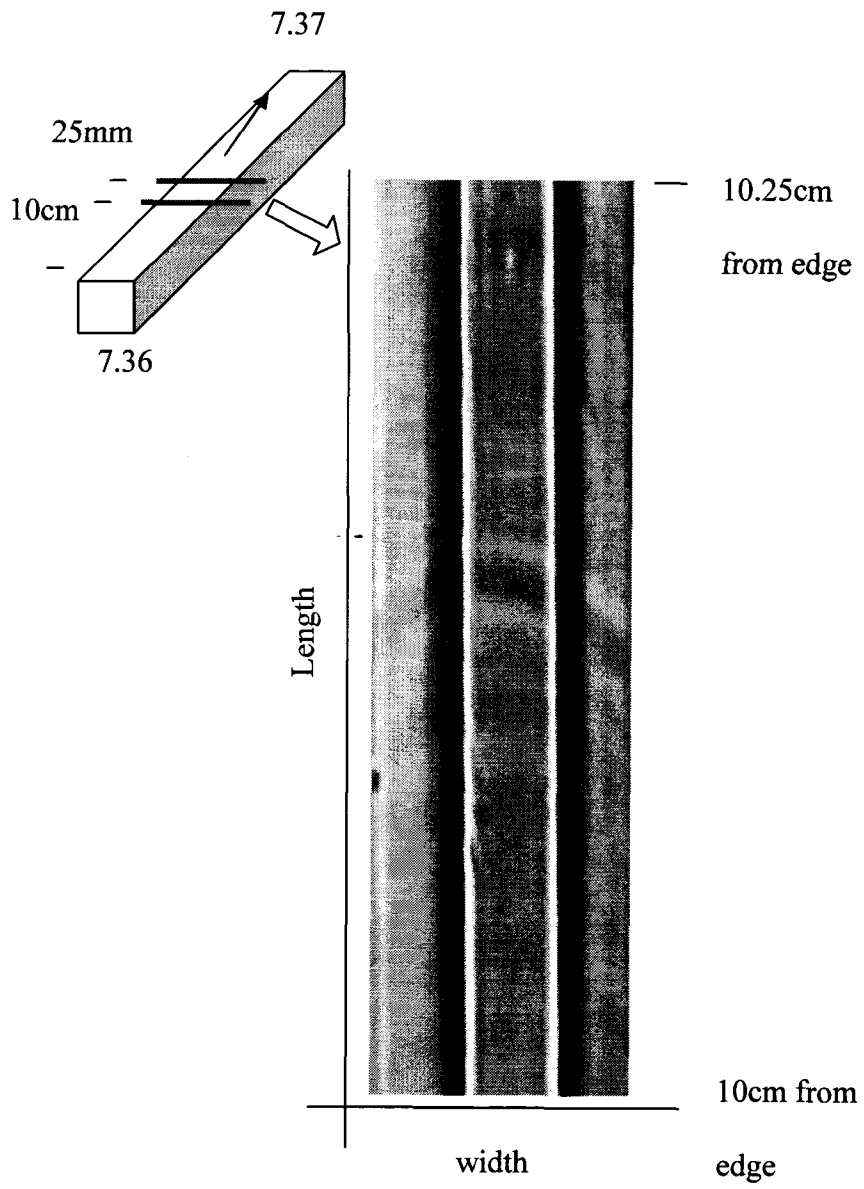
Figure 4.3.1-1 C-scan of the 7.37 FSW sample.
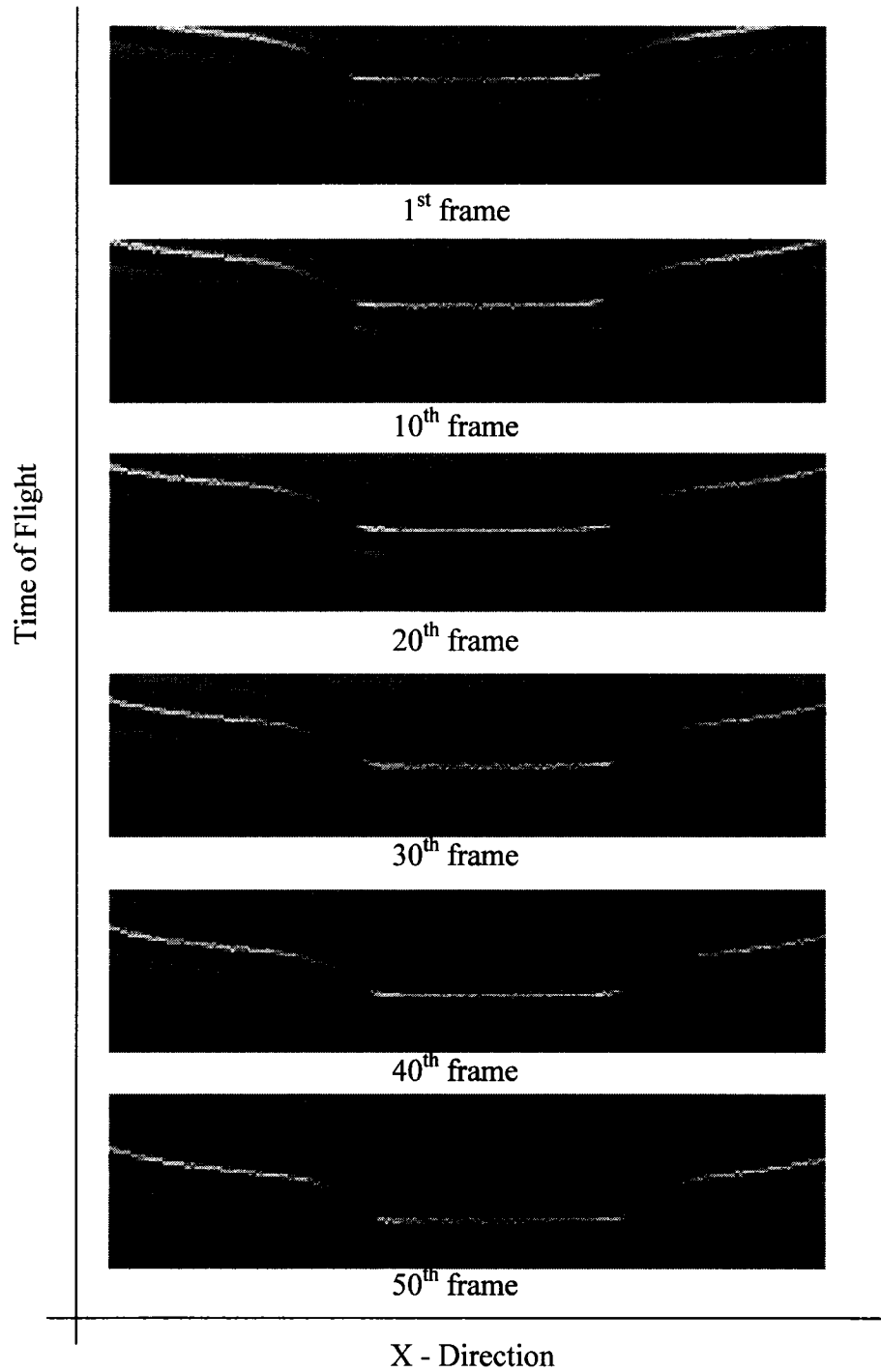
Figure 4.3.1-2 B-scans of 7.37 FSW sample scanned in the portion 10cm from the edge with a length of 25mm and composes of 50 frames; 1st, 10th, 20th, 30th, 40th and 50th frames.

46

The B-scan images did not show any cracks similar to the optical images made by destructive testing. Considering the location and height of crack mentioned in those results, we focused on observing changes in same location but did not find any significant changes in the B-scan images. The reason is probably the crack maybe too small, 0.39mm to be exact or the crack is not present in this sample.
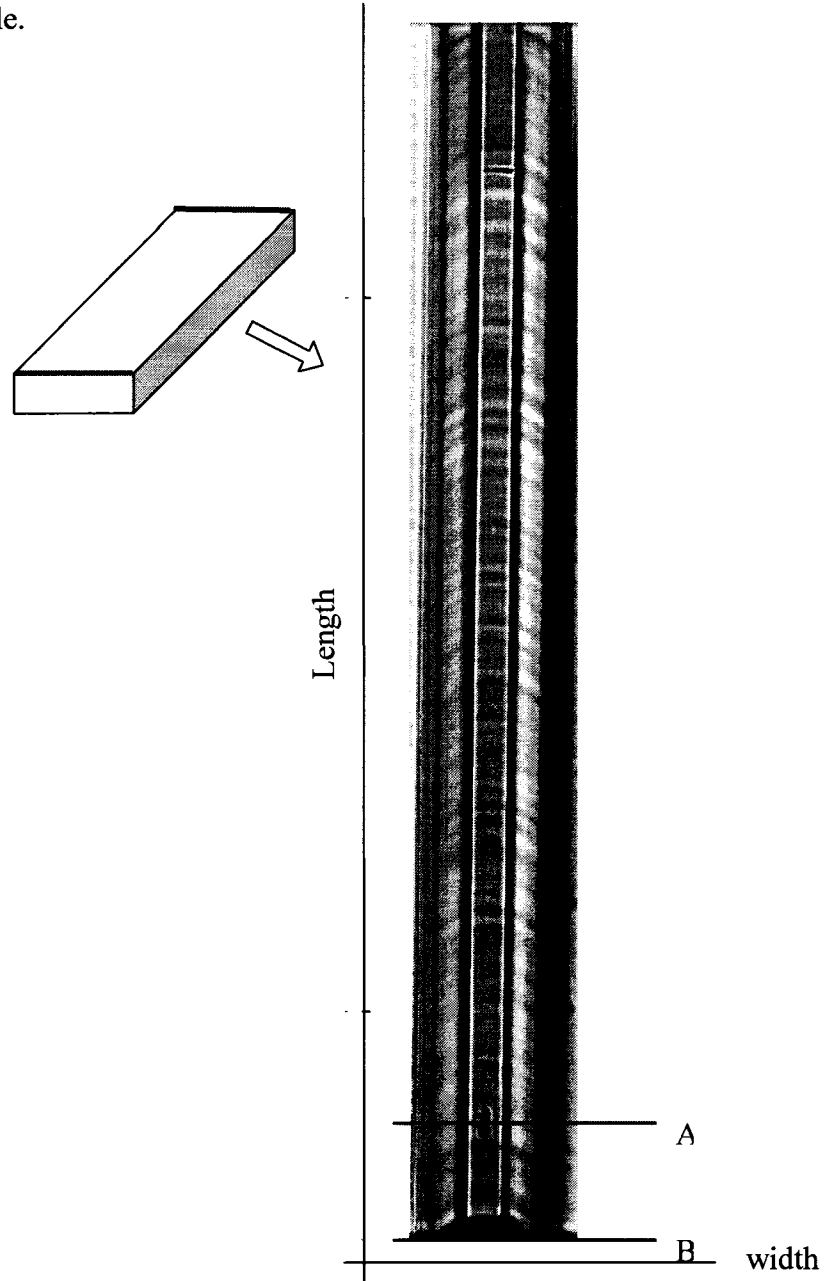
Figure 4.3.1-3 C-scan of the small FSW sample scanned from the edge to edge, approximately 13cm in length.

47
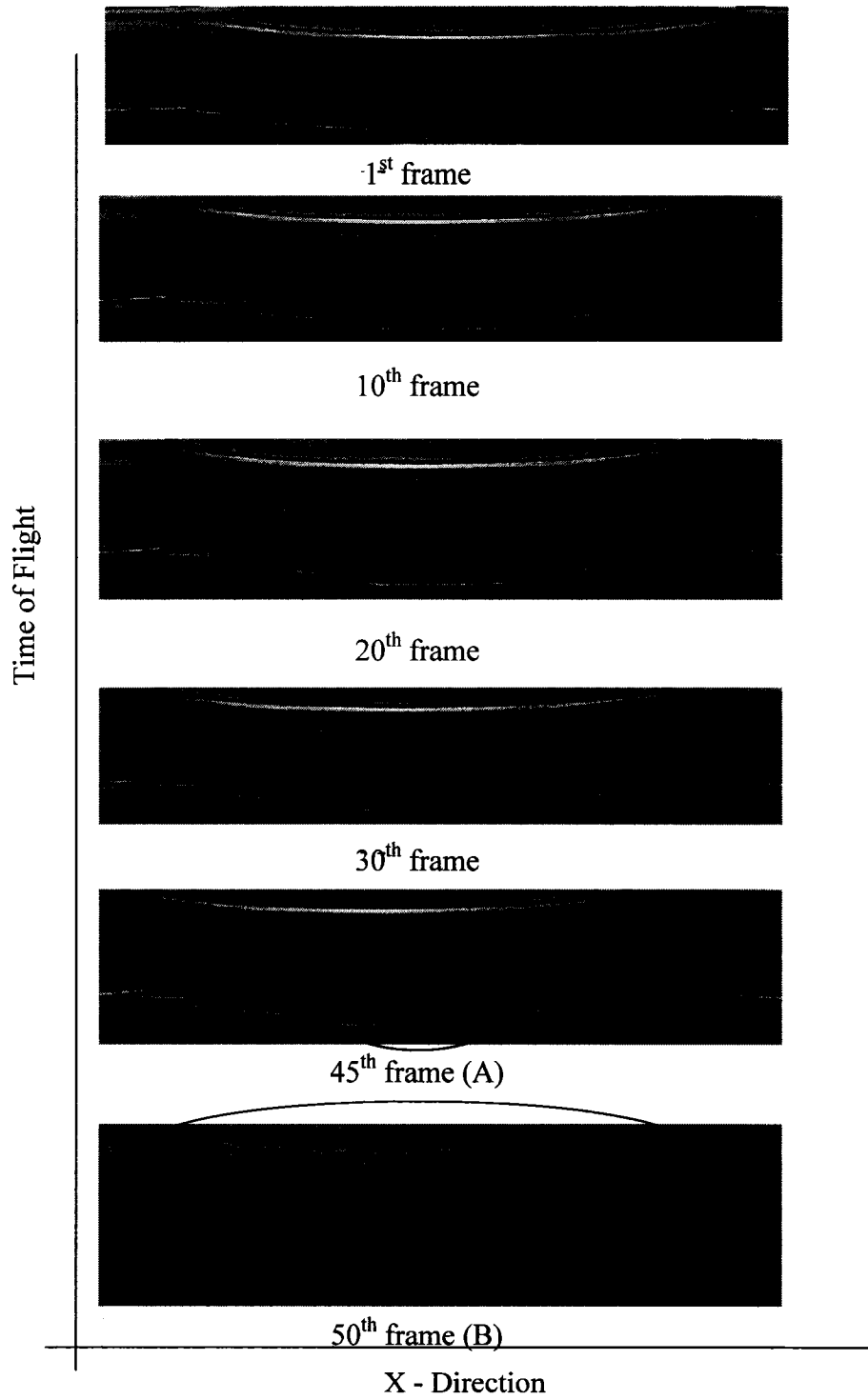
Figure 4.3.1-4 B-scans of small FSW sample scanned from edge to edge with a length of 13cm; 1st, 10th, 20th, 30th, 45th and 50th frames.

48

In this sample, 2 significant observations were recorded. First, on the 45th frame, it showed the abrupt change because of the spot present on the weld line curve of the FSW sample. Secondly is that on the 50th frame, it shows the delamination part. This was confirmed by visual inspection. These B-scan images proved that ultrasound inspection can detect cracks inside FSW weld line but this delamination appeared parallel to the inspection surface that is why it became possible to detect. But still, other cracks such as root cracks were negative results.

49

4.3.2. Results from Single Element

The images below are side by side comparison of a normal beam bscan and an angled beam bscan using single element transducer.

Time of flight

x- direction
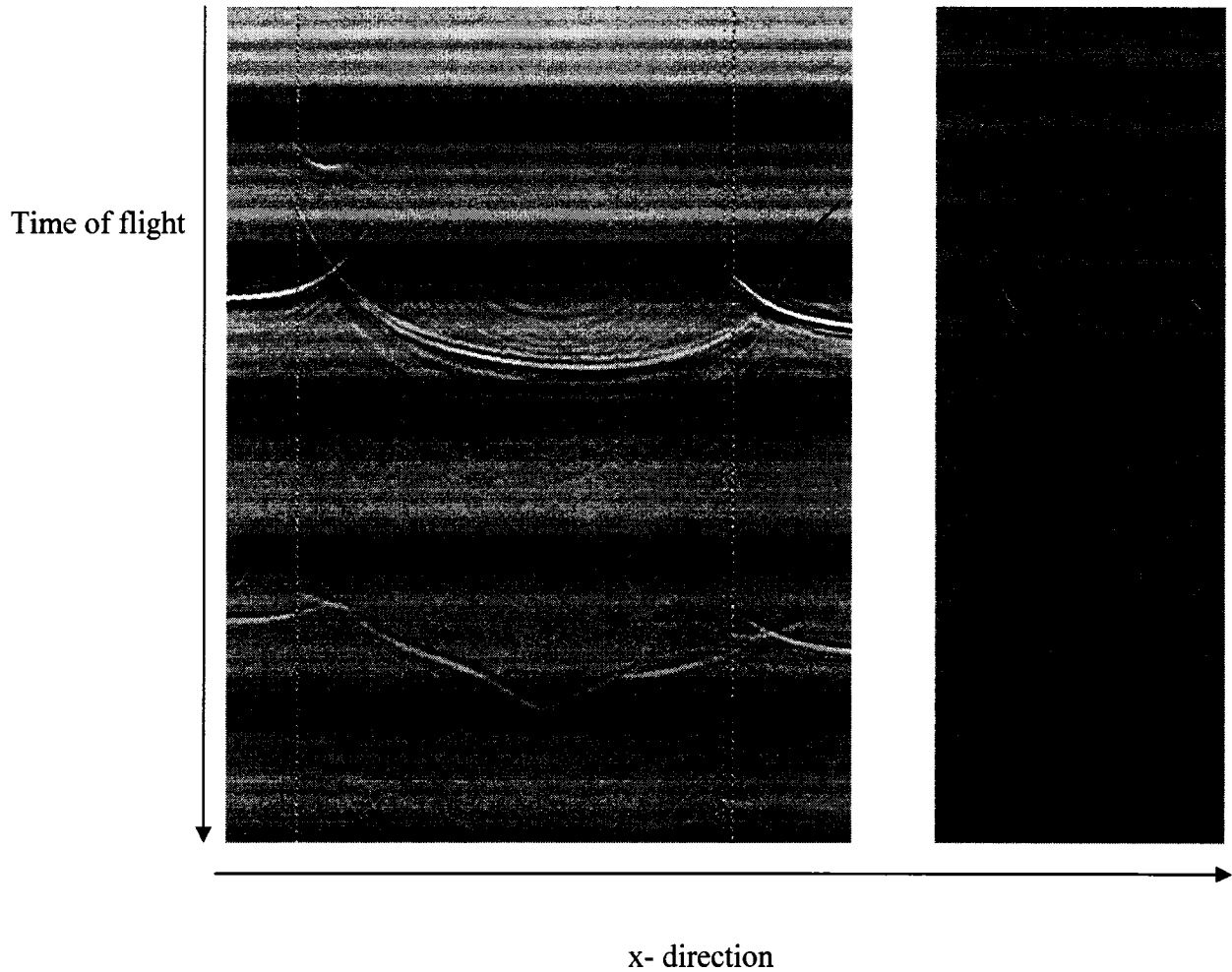
Figure 4.3.2-1 B-scan of the aluminum FSW sample, normal beam and angled beam.

The reflections of from the angled beam B-scan image corresponds the positions of the reflections with the B-scans gathered by using normal beam. This comparison was done to inspect any unusual reflection that might appear in angled beam images that might indicate the presence of a root crack. The B-scans above doesn't show any significant response that might be predicted as root

50
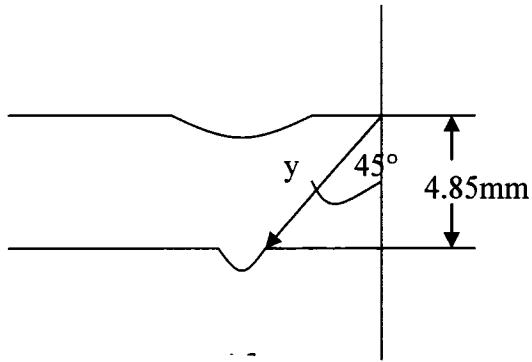
crack. But looking at the B-scan below, it gives multiple reflections (black arrows) from the region where root crack usually appears. This was proven by the computation done using time of flight principle. The time delay corresponds to the distance from the top surface of FSW to the bottom of the curve like bump.

$$y = \cos 45° * 4.85mm$$
$$y = 6.85mm$$

Which when you compute time delay will be equal to:

$$t = \frac{2 * 6.85mm}{3200m/s}$$
$$t = 4.285 \mu s$$
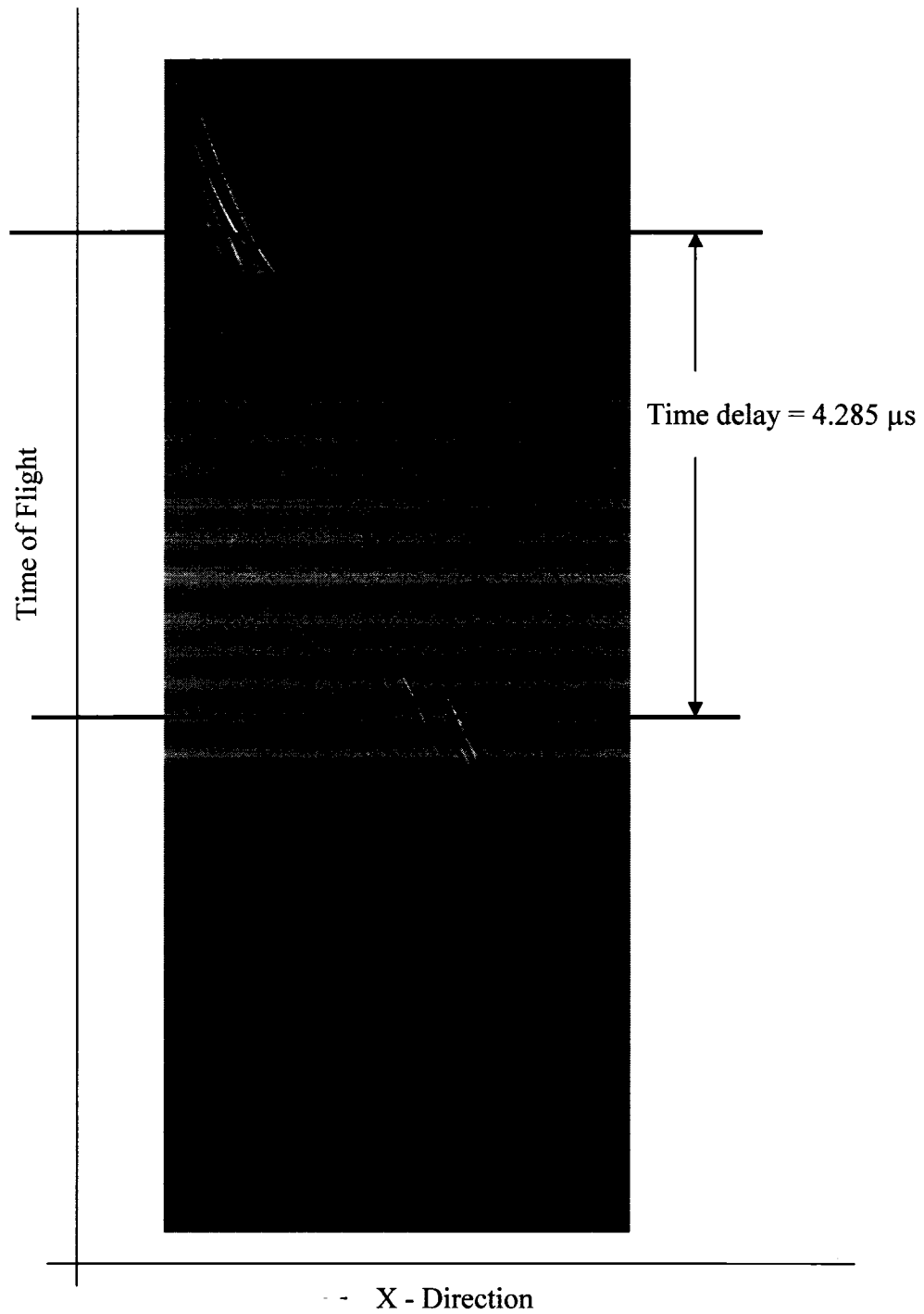
Figure 4.3.2-2 B-scan of the aluminum FSW sample with multiple reflection.

4.3.3. Results from R/D Tech OmniScan

Since it was proven that angled beam inspection is more appropriate in detecting root cracks through inspection using single element transducer, array probes were used to compare improvements in detection. The following shows the S-scan of the samples using 10MHz, 32 element array transducer with 45 degrees sound beam and scans from 15 to 30 degrees over the material. First was the synthesized sample. It is very clear from the S-scans that the notch created was very visible in this kind of inspection set-up. The noticeable improvement was that there was no need for the probe to be moved to be able to cover the 3 reflectors. In one position, it provides all the reflections that were the point of interest in this scenario. Also, there was a big improvement in the resolution due to the combined energy from the synchronized pulses coming out from each element. It offers a higher signal to noise ratio compare to single element.

Inspection with 32 Element Array Transducer

Inspection set-up

Transducer: 32 element 10MHz array transducer
Specimen: Aluminum Sheet, 4.5mm thickness
Immersion Technique
Sectorial Scan from 15° to 30°
Incident Wave: Longitudinal Wave at 20°
Refracted Wave: Shear Wave at 45°

Without notch

Y- parameter e.g.: depth in y axis

X- parameter e.g.: distance in x direction
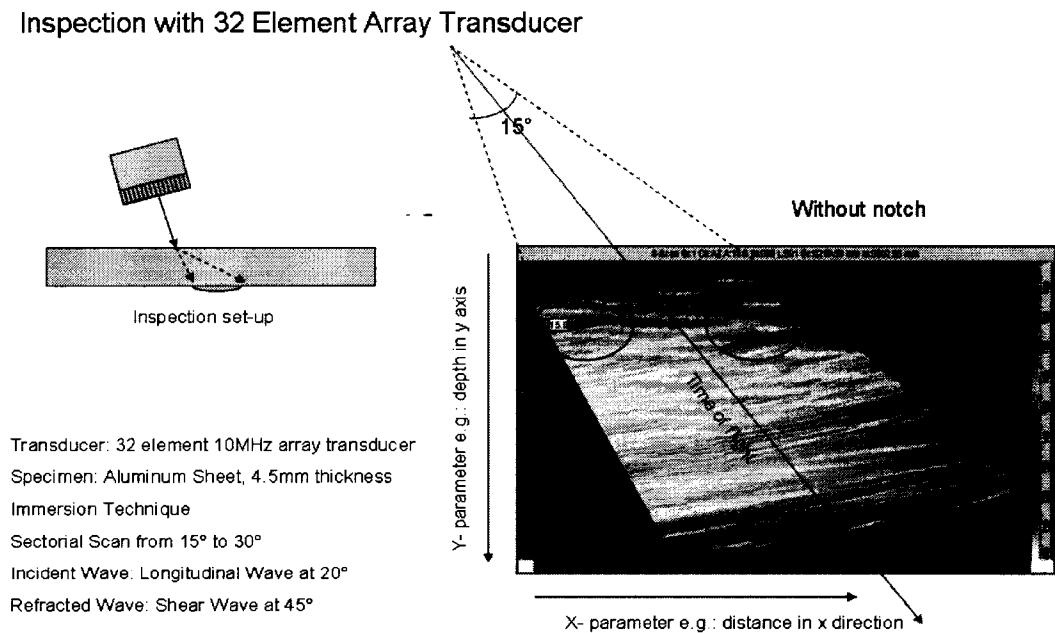
Figure 4.3.3-1 S-scan of the aluminum synthetic FSW sample without notch.

53

Inspection with 32 Element Array Transducer

Inspection set-up

15°

With notch

Y- parameter e.g.: depth in y axis

X- parameter e.g.: distance in x direction

Transducer: 32 element 10MHz array transducer
Specimen: Aluminum Sheet, 4.5mm thickness
Immersion Technique
Sectorial Scan from 15° to 30°
Incident Wave: Longitudinal Wave at 20°
Refracted Wave: Shear Wave at 45°
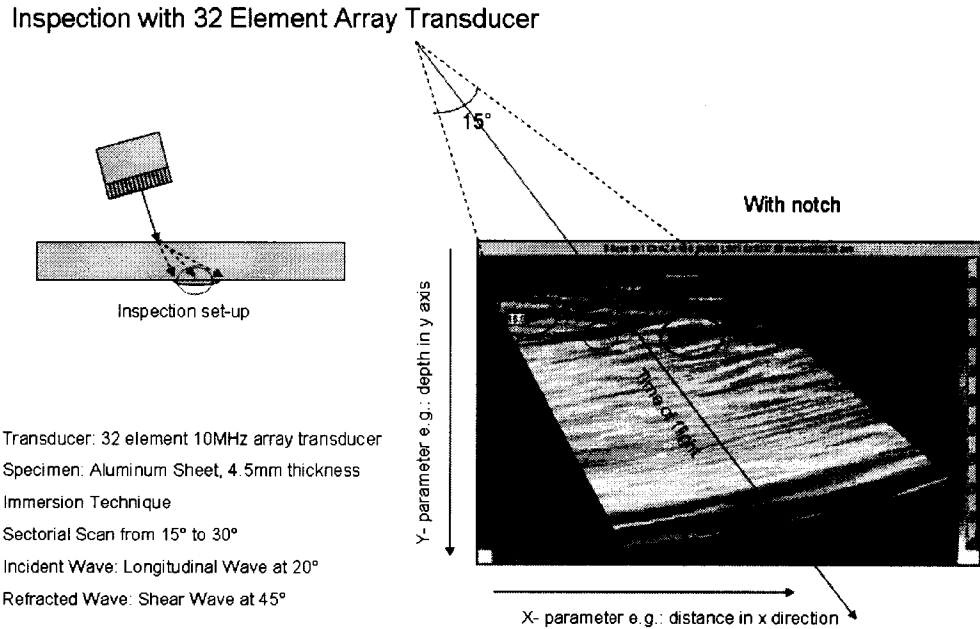
Figure 4.3.3-2 S-scan of the aluminum synthetic FSW sample with notch.

Moving on to the real FSW sample was a lot more confusion. Due to the metallurgical changes or the changes in the grain structure of the aluminum caused by the unique FSW process, a lot of un-interpretable signals came out of the monitor. In addition, rough surface makes the signals distorted plus the thought that maybe there is really no crack present on the samples. The signals acquired were analyzed as follows. B-scan is taken the other way around, the sample facing upside down. And the image appeared like this:

Figure 4.3.3-3 B-scan of the FSW sample scanned upside down
(Time of flight vs. x-dimension).

54

From this image, the assumption that the weld line would create a curve like bottom, it seems that this specific sample is not. So, the signals may come from these reflectors as shown below.
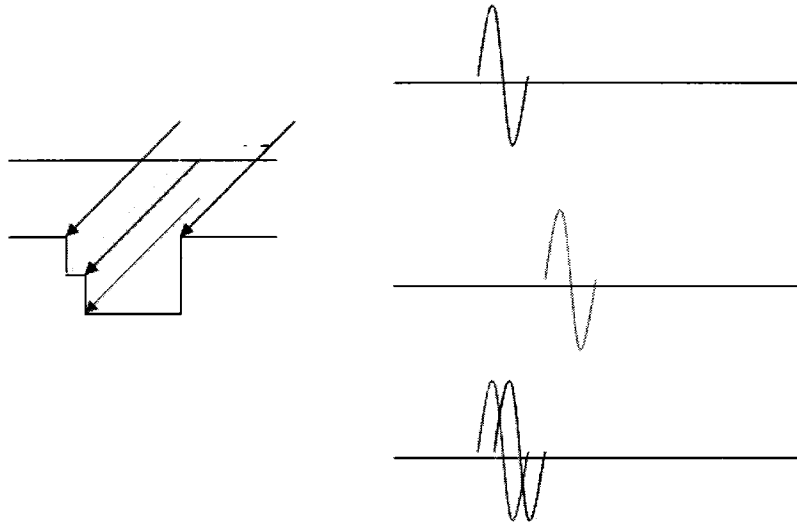
Figure 4.3.3-4 Predicted reflectors from FSW 2nd batch of samples,
Illustration of their time delays according to distance.

This assumption is validated with the use of the phased array technology and by using Omniscan device and the results provide a similar output.
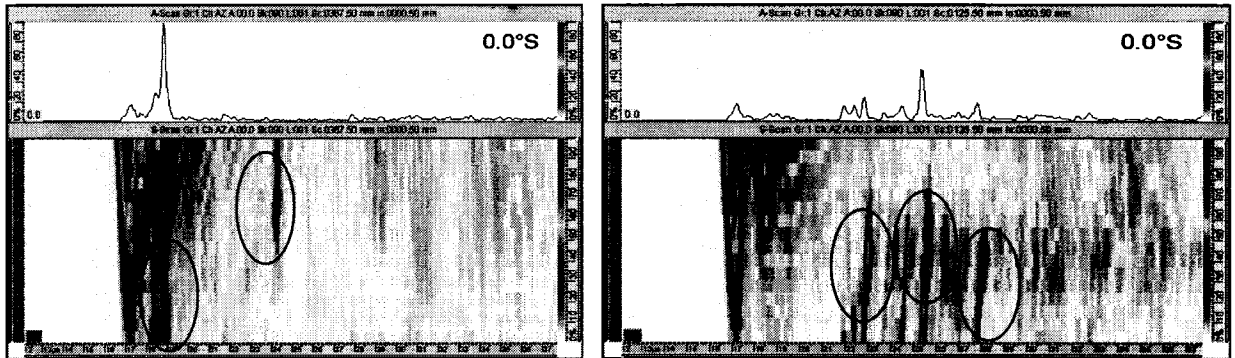
Figure 4.3.3-5 S-scan from reflectors shown in fig 4.3.3-4.

55

The next images also correspond to same reflectors from same samples but are just viewed differently but still using array probe and Omniscan device and same transducer. The settings of the acquisition device are just different from the settings above but give the same information.
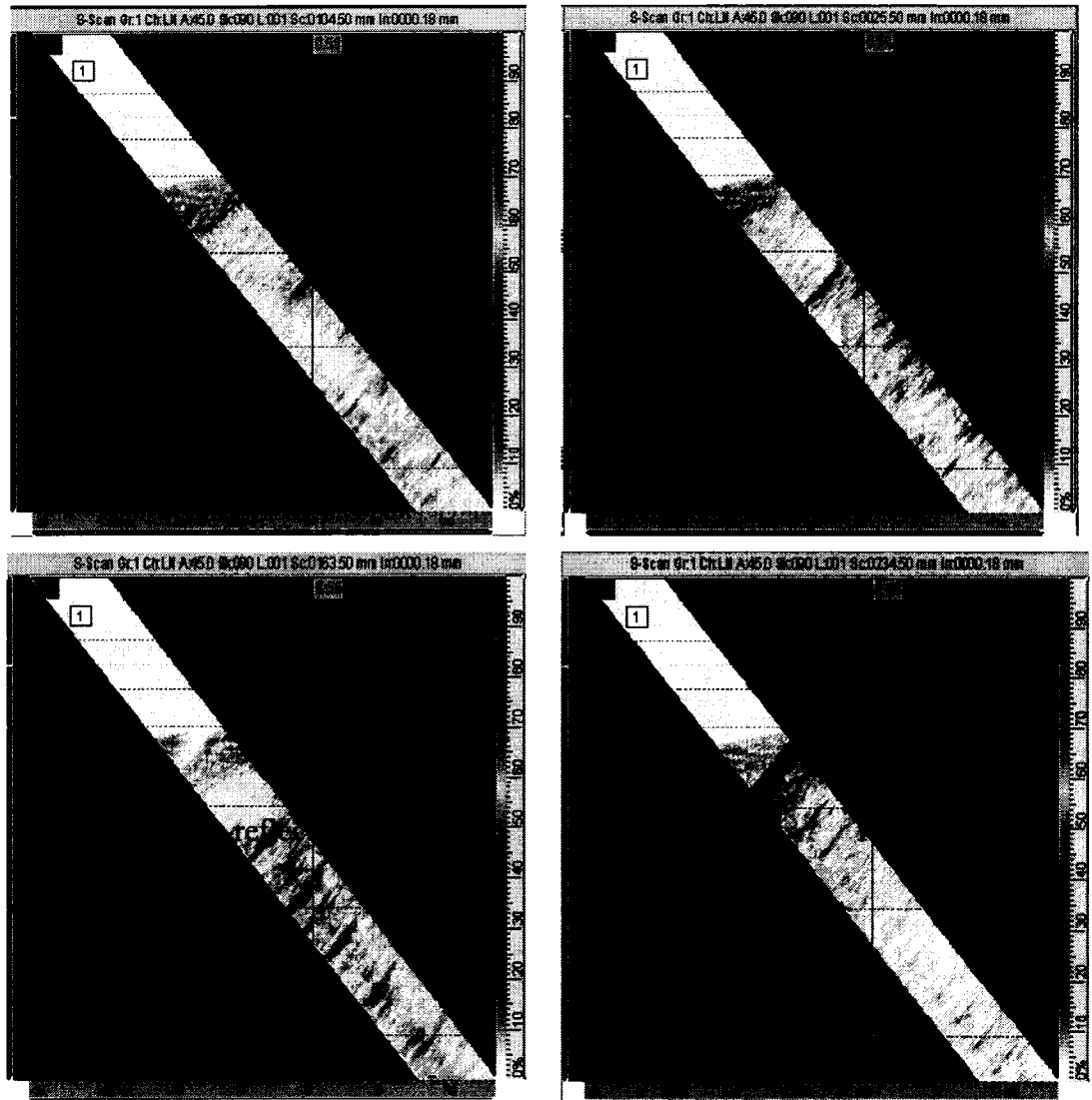
Figure 4.3.3-6 Different S-scan view from reflectors.

56

4.3.4. Summary of Experimental Results

The synthetic sample was investigated using all the methods mentioned above. Investigation was done with different crack depths then measuring the signal-to-noise ratio. The detection capability is evaluated by determining what transducer can detect the smallest crack depth. Signal-to-noise ratio is measured and the results are shown on the table below. Even though the accuracy of the SNR estimation is low, all setups are sensitive enough to detect cracks larger 50μm.

Table 4.3.4 Sensitivity measurement of different inspection systems used.

	200-100 μm	100-70 μm	70-50 μm	<50 μm
V2098	20-14	10-4	15	1
32 elem R@D	25-20	10-6	3	2
matrix 15 MHz	15-6	11-3	4-2	-

57

CHAPTER V

SIGNAL PROCESSING TO ENHANCE DEFECT DETECTION

5.1. Signal Processing Applied in Ultrasonic

The utilization of signal processing techniques in nondestructive testing, especially in ultrasonics, is widespread. Signal averaging, matched filtering, frequency spectrum analysis, neural networks and autoregressive analysis have all been used to analyze ultrasonic signals. The Wavelet Transform is the most recent technique for these kinds of application.

Conventional filtering techniques were used to enhance flaw detection in ultrasonic signals, such as matched filtering and Wiener filtering (Bilgutay *et al.*, 1981). Wiener filtering relies on statistical differences between the spectral magnitudes of the flaw and noise. In this case, it is assumed that the echoes due to flaw differ in spectral content from echoes due to background noises. Unfortunately, this filter requires a priori knowledge of the power spectral density characterizations of both the noise and flaw echoes. Match filtering, in another case, is also effective but not unless you know the signal shape of the expected flaw. The need for deterministic model for the flaw echo limits the application of match filter to flaws composed of single dominant scatterer. Both of these techniques, together with some other filtering that were used in this scenario, the signal is analyzed either in time domain or in frequency domain but never on both. In ultrasonic flaw detection the ultrasonic signal is usually a broadband pulsed modulated at the center frequency of the transducer; therefore transient signal is usually time and frequency limited. With this, the utilization of 2 dimensional analyses can be more appropriate.

Xing Li *et al.* studied enhancement of flaw detection in ultrasonic signals by using Split Spectrum Processing (SSP) which is based on the STFT time-frequency decomposition (Li, et al., 1992). The input signal is transformed into frequency domain by Fast Fourier Transform. The resulting spectrum is split into numbers of narrowband spectra by passing into passband filters. The narrowband spectra is processed back into time domain with Inverse Fourier Transform and weighted such that the amplitude of

58

each narrowband signal is normalized to unity. Then the results are processed more using some nonlinear processing to reduce noise contribution and extract the flaw information. Several techniques have been employed for processing the signal obtained from original wideband echo signal. Some of these are average of squared signals, squared of average signals and minimization algorithms. M.M Bilgutay et al, used all these three techniques to compare which one provides a better signal-to-noise ratio on the output signal and proves that the minimization algorithm give the best output.

Average of squared signals is obtained by normalizing, squaring and then averaging the signals corresponding to different frequency bands. If we define $r_i(t)$ as the filtered and normalized signal corresponding to the *ith* band centered at frequency f_i, then the output of the averaging algorithm is given by:

$$y(t) = \frac{1}{m} \sum_{i=1}^{m} r_i^2(t)$$

where m is the number of frequency shifted signals. Squared of average signal is an alternate averaging technique which averages the normalized signals corresponding to the different frequency bands and squares the resulting signal giving:

$$y(t) = \left[\frac{1}{m} \sum_{i=1}^{m} r_i(t) \right]^2$$

The minimization technique represents the reflection at each range by the minimum amplitude appearing at that corresponding range in any of the m filtered, normalized, and squared signals. The output for the minimization algorithm may be defined as

$$y(t) = \min_i \left[r_i(t); i = 1,2,3...m \right]$$

Utilizing these three techniques, comparisons of an ultrasonic signal output is shown below and is proven that minimization has dramatically enhanced flaw detection.
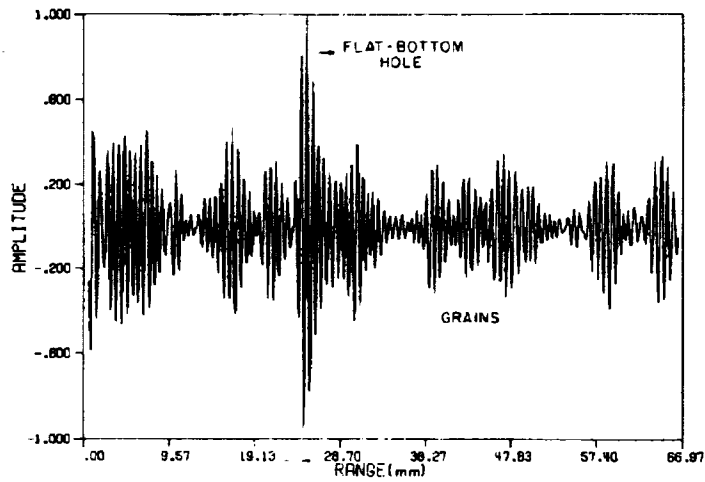
59

Figure 5.1-1 Ultrasonic Signal from Titanium with 1.19 mm diameter flat-bottom hole.
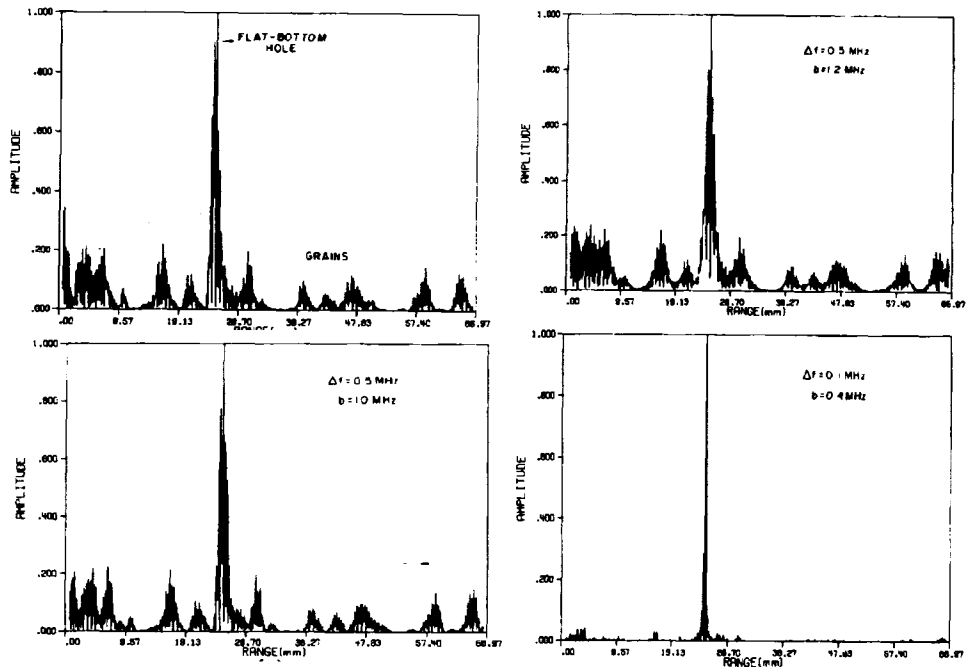

Figure 5.1-2 Output of the nonlinear techniques: a.) averaged signal of fig 3.3.-1; b.) averaged of squared signal; c.) square of averaged signal and d.) square-minimization algorithm.

(Figures from "Spectral Histogram...by Li")

60

This process is analogous to Wiener Filtering mentioned above. However, unlike Wiener Filter, the nonlinear minimization algorithm can be used to determine the spectral region with high SNR without any a priori knowledge. The output SNR versus frequency range was evaluated for minimization and Gaussian shaped bandpass filter, bandwidth center at 3.3MHz. The original signal was obtained using a broadband transducer of 100MHz (Li, et al., 1992).
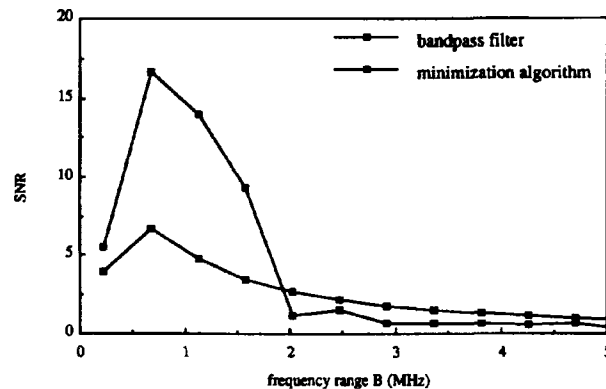
Figure 5.1-3 Performance comparison of bandpass filter and minimization algorithm.

Figure 5-3 indicates that the frequency diverse statistic filter, minimization algorithm, generally outperforms the bandpass filter in the high SNR frequency regions. However, if the processing frequency range is too large, the performance of the minimization algorithm will fall below that of the bandpass filter.

The passband filters used in SSP decomposition have constant absolute bandwidth, which in many cases is not optimal representation for ultrasonic signals obtained using wideband transducers in the pulse-echo mode.

5.2. Aim in Using Signal Enhancement

In materials made by FSW, there maybe lots of sources of un-interpretable pulses, aside from the fact that ultrasound testing systems are noisy by nature. This noisiness may come from internal sources, such as grain structures of the material or externally such as noises produced from the transducers and an amount of electrical noise from the acquisition system. The ensemble of these noise echoes limits the detection of small tight cracks, flaws or other metallurgical defects. Usually, the reflection from small

61

cracks such as root crack in FSW initiate a very small amount of amplitude which might appear hidden in the background noises. It gives us a very small amount of signal to noise ratio which confines the sensitivity of our test scheme. The main goal in this utilization of DWT in FSW signals is to suppress the noise as much as possible at the same time limiting the loss of defect information.

In many instances, the measured ultrasonic signal $s(t)$ can be expressed as the sum of two components (Abbate *et al.*, 1997):

$$s(t) = \bar{y}(t) + n(t)$$

where $y(t)$ is the acoustic signal of the crack embedded in the noise $n(t)$. The signal $s(t)$ is thus band-limited, corrupted and distorted by noise. Most of the studies, they represent ultrasound noise to be Gaussian additive noise because the impulse response coming out of ultrasonic transducer has an envelope of a Gaussian function. Meaning the noise that it produces came out to have the same impulse shape. The purpose of this work is to obtain another signal $s^R(t)$ as close as possible to $y(t)$, thus minimizing the effect of $n(t)$. This assumption, that equation above is a linear function, was chosen to avoid complexity.

Symbolically, consider Figure 5.2-1. The top image shows a noisy image. At first, it seems that there is no significant pulse that may indicate a crack but as it was enhanced by a signal processing technique, DWT noise suppression; it shows two pulses which gives the information about the cracks.
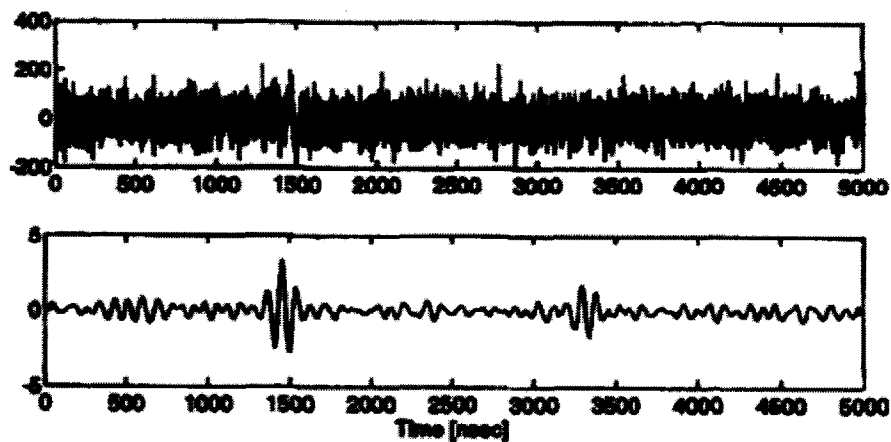

Figure 5.2-1 DWT Noise Suppression of an ultrasonic signal. *(Figures from Ref. #21)*

62

5.3. Wavelet Transform for Root Crack Detection

5.3.1. Motivation on Wavelet Transform

Transforming the signals from one domain to another is not new in signal processing field. These transformations are done to gather data that are not present in the original domain of the signal. One of the most popular and most used transformations is Fourier Transform. Fourier transform decomposes the signal into sum of sinusoids of different frequencies. It provides a frequency versus amplitude representation of the original signal. It is mathematically represented as:

$$X(f) = \int_{-\infty}^{\infty} x(t)e^{-2j\pi ft} dt$$

where f is frequency, t is time, $x(t)$ is the time domain signal and $X(f)$ is the Fourier Transform of $x(t)$. The drawback of this transform in this application is that, it works more effectively for stationary signals. It can also be used for non-stationary signals but if only interested in spectral components, not their time of occurrence. In our case, the A-scans that we are getting are non-stationary and we are interested in the time of occurrence of the spectral components of the signal.

Short Time Fourier Transform (STFT) was then developed to solve the Fourier Transform's limitations. STFT provides accurate information about the signal simultaneously in the time domain and the frequency domain. It provides a Fourier Transform of a function as examined through some time-limited window centered on a certain time, t.

$$STFT(\tau, f) = \int_{-\infty}^{\infty} x(t)w(t - \tau)e^{-j2\pi ft} dt$$

where $w(\tau)$ is the window function. The STFT analysis has the same resolution at all locations in time-frequency-plane, due to the fact that the same window is used over the entire frequency range (Stark, 2005).
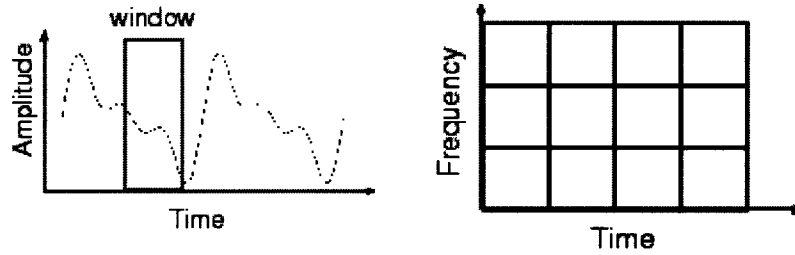
63

Figure 5.3.1-1 STFT Windowing Process.

(Figures from www.mathworks.com)

The choice of the window size thus determines the resolution of the analysis in the time and frequency domains. If the window is too narrow, it provides good time resolution but poor frequency resolution. But if the window is too wide, it gives good frequency resolution but poor time resolution. This problem was solved by applying Wavelet Transform.

Wavelet Transform (WT) is a recently developed method of processing transient non-stationary signals simultaneously in time and frequency domains. It breaks up the signal into shifted and scaled version of the mother wavelet – a finite length or a fast decaying waveform (Abbate et al., 1997). It is used to extract details and information on time and frequency domains from the transient signal under analysis. In this transform, the width of the window is changed as the transform is computed for every single spectral component. In this approach, it results in a more natural description of the signal, since the size of the window in the time domain is now a function of scaling. By definition, the WT is the correlation between the signal and set of daughter wavelets that was originated from the mother wavelet. Mathematically, Wavelet transform of a function, $W_{(a,b)}$ is defined as:

$$W_{(a,b)} = \int_{-\infty}^{\infty} x(t) h_{a,b}(t) dt$$

$$h_{a,b}(t) = a^{-\frac{1}{2}} h\left(\frac{t-b}{a}\right)$$

64

where $h_{(a,b)}(t)$ is the mother wavelet, a means dilation and b means shifting.
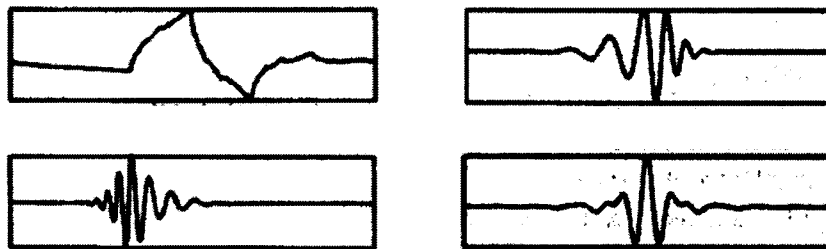
Figure 5.3.1-2 Examples of mother wavelets. Daubechies 2, Daubechies 10, Vaidyanathan and Battle-Lemarie *(Images from Ref #23)*

The normalization constant $a^{-1/2}$ was chosen such that every daughter wavelet has identical energy. - -

As with any transformation schemes, an inverse wavelet transform (IWT) can be defined as: (other variables have same value as WT)

$$IWT = \int_{-\infty}^{\infty} \int_{-\infty}^{\infty} W_s(a,b)h_{a,b}(t)\frac{da}{a^2}db$$
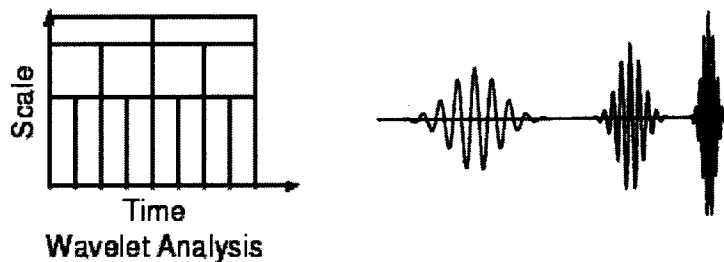
Figure 5.3.1-3 Wavelet 2-Dimensional Analysis; Wavelet Scaling.

(Figures from www.mathworks.com)

65

5.3.2. Multi-Resolution Analysis

Wavelet Transform can be seen as having a bank of filters which are constructed by scaling of function $h(t)$. The filter that is constructed by dilated version of mother wavelet processes low frequency information of signal $s(t)$ and calls the results as approximations, and the filter related to compressed version analyzes the high frequency information and calls the results as details. So the output of the WT is also dependent on the mother wavelet used. The illustration of the discrete wavelet transform is shown below. The high-pass filtering is equivalent to the compression and the low-pass filtering is the dilation process. Downsampling is necessary to avoid redundancy. Also, the reconstruction part is basically following the same process inversely. Instead of downsampling, upsampling is needed this time. The high-pass and low-pass filters are as much as possible having behavior close to the high-pass and low-pass filter in the decomposition process but not necessarily identical.
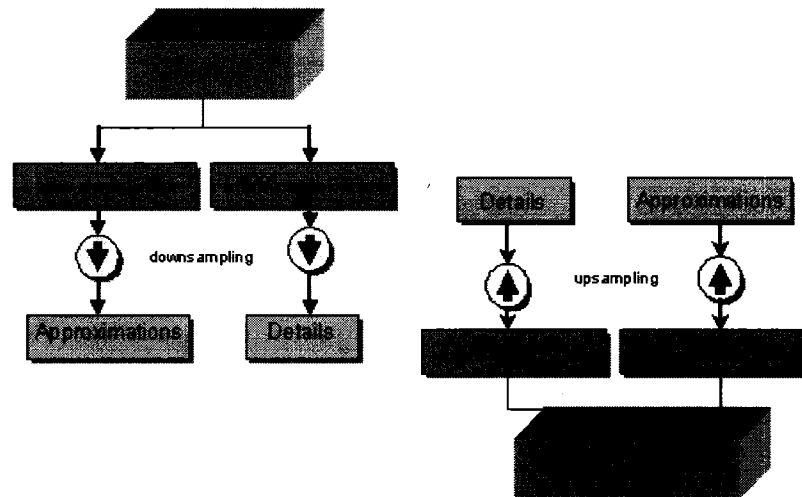

Figure 5.3.2-1 Signal Decomposition and Signal Reconstruction.

For multi-level decomposition, the signal is run thru the bank of filters not just once, but up to the level of interest that might give you the best output in a certain application.

66
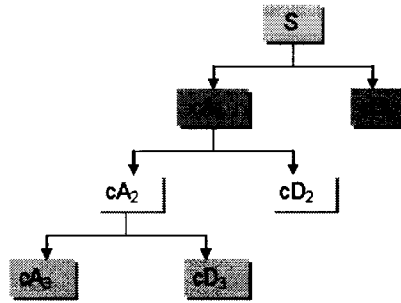
Figure 5.3.2-2 Multi Decomposition Stages.

The signal S is equal to: $S = cA_3 + cD_3 + cD_2 + cD_1$.

5.3.3. Wavelet Noise Suppression Algorithm
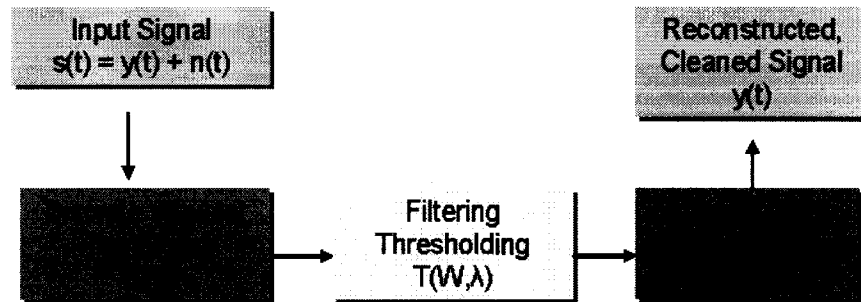
Figure 5.3.3-1 Wavelet noise suppression algorithm

From the original A-scan, the signal was transposed using Wavelet Transform followed by the thresholding scheme. Threshold value is determined depending on every application. After DWT decomposition, noise is spread out (decomposed) over all the DWT coefficients. The noise level is not too high and its coefficients are lower. On the other hand, the coefficients contributed by the signal of interest are relatively larger so that we can recognize the signal and the signal wavelet coefficients. It is very important to determine the best value of threshold because if it is too low, the defect will not be reported. In this application, the threshold value is computed based on statistical analysis as follows:

67

$$\lambda = \sigma \sqrt{2x \log N}$$

where N is the number of DWT coefficients and σ is the variance of DWT coefficients in each level.

Global threshold is popularly used for wavelet coefficients thresholding. In this study, level-dependent threshold values were also adopted to improve the performance of the method. Instead of using a global threshold, level-dependent thresholding uses a group of thresholds, one for each scale level. And thresholding is done in soft thresholding manner summarized below:

$$T(W,\lambda) = \begin{cases} sign(W)x(\|W\| - \lambda) & if \, \|W\| > \lambda \\ 0 & otherwise \end{cases}$$
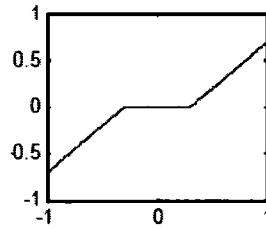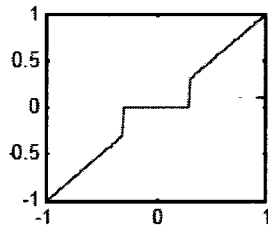
$$T(Y,\lambda) = \begin{cases} Y & if \, \|Y\| > \lambda \\ 0 & otherwise \end{cases} \qquad \begin{cases} sign(Y) \times (\|Y\| - \lambda) & if \, \|Y\| > \lambda \\ 0 & otherwise \end{cases}$$

Figure 5.3.3-2 Wavelet Noise Suppression Thresholding Schemes
(Figures from Ref. #24)

After thresholding process, like any other transform process in signal processing, we have to return it back to the original form. So we applied Inverse DWT to reconstruct the filtered signal. Finally, the result will be a cleaned signal eliminating some unwanted noise from our acquired A-scan.

68

5.4. Results and Discussions

The next illustration shows a real ultrasonic pulse from a root crack of an FSW specimen using 4 different kinds of mother wavelet. From the signal acquired directly from FSW, it is difficult to identify the root crack because of too much noise and very low amplitude coming from the defect. But with the proper choice of mother wavelet to use, we can drastically reduce the amount of noise and be able to detect the pulse from the root crack.
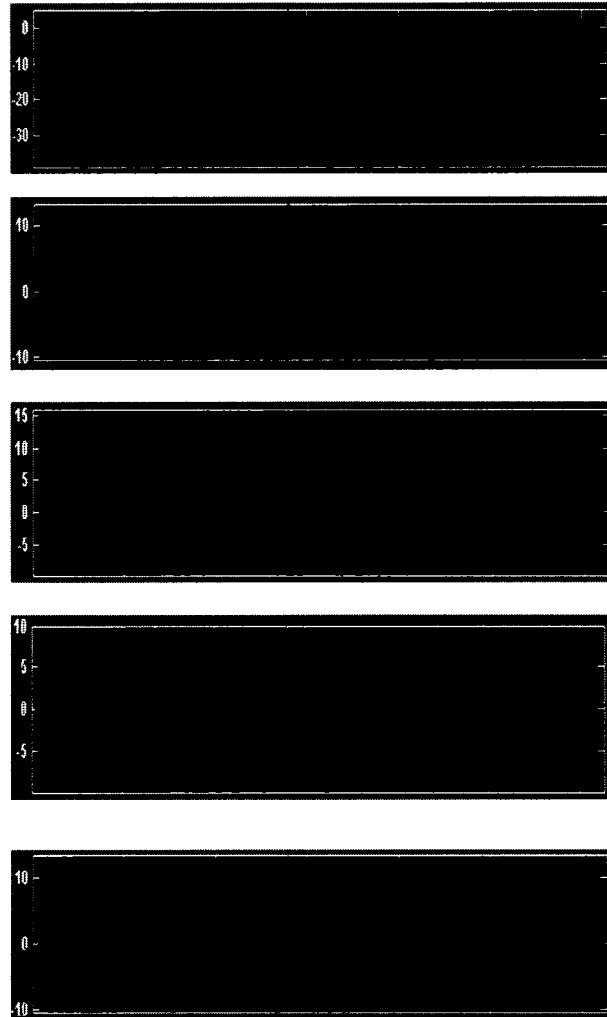
Figure 5.4-1 Denoised root crack pulse using different mother wavelets;
Daubechies 10, Coiflet 8, Symlet 8 and Dmey.

69
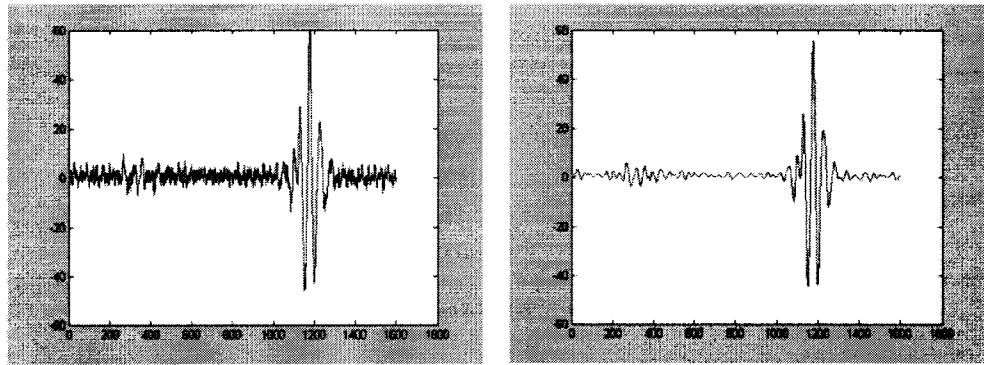
Figure 5.4-2 Denoised using db10 at level 4; transducer: V2098, 15MHz.

After using different kinds of mother wavelet, the result shows that Daubechies 10, Symlet 8, Coiflet 4 and Discrete Wavelet Meyer, are four of the mother wavelets that provides the best similarity with the crack pulses, the reason why they filtered the noise significantly. This is because this four wavelet function is the most similar to the ultrasonic crack echo and the higher the similarity, the higher the amplitude of the DWT. That is why the crack echoes are enhanced more than the other portions of the signal. Compare the following result below to the results of the 4 wavelets above. The signal is not fully enhanced because the Haar and Reverse Bio-orthogonal wavelet is not that similar to ultrasound crack response. Therefore it will still give a low signal-to-noise ratio.
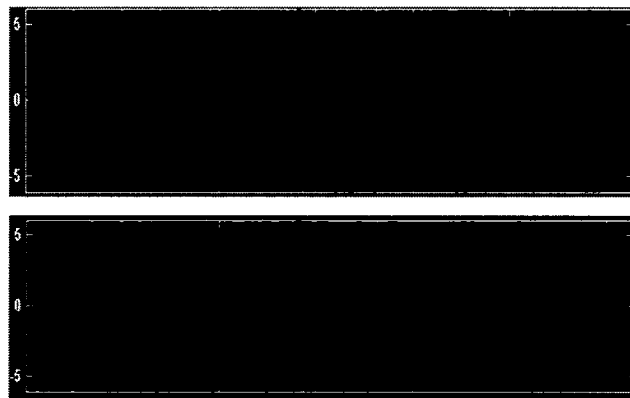
Figure 5.4-3 Denoised using Haar and Reverse Bio-Orthogonal wavelet.

70

Table 5.4-1 Efficiency of different mother wavelets in root crack detection.

Daubechies 2	-
Daubechies 4	--
Daubechies 10	----
Symlet 2	-
Symlet 8	----
Haar	x
Coiflet 1	x
Coiflet 4	----
Rbio 1.1	x
Rbio 2.8	-
Dmey	----
Bior 1.1	x

Legend:　　x　　inefficient

　　　　　　-　　good

　　　　　　--　　better

　　　　　　---　　best

　　　　　　----　　most efficient

The table above shows some comparison of different kinds of wavelet. This efficiency was based from the results and experimental observations. Number of dash lines determines the effectiveness, the higher the better, and x marks means it is not advisable to use this wavelet in root crack detection. As mentioned, those mother wavelets that are not similar to crack responses gave poor output.

The signal-to-noise ratio improvement was measured and calculated as a ratio of the input SNR and the output SNR. The improvement is summarized on Table and graph below. Notice that all of them results a better SNR.

71

Table 5.4-2 Improvement of Signal-to-Noise Ratio.

SNR in (dB)	SNR -out (dB)			
	db10	sym8	coif4	dmey
-25	0.3	0.8	0.4	0.8
-20	2	3	1	1
-15	3	7	3	2
-10	7	8	4	3
-5	10	9	7	6
0	13	10	10	9
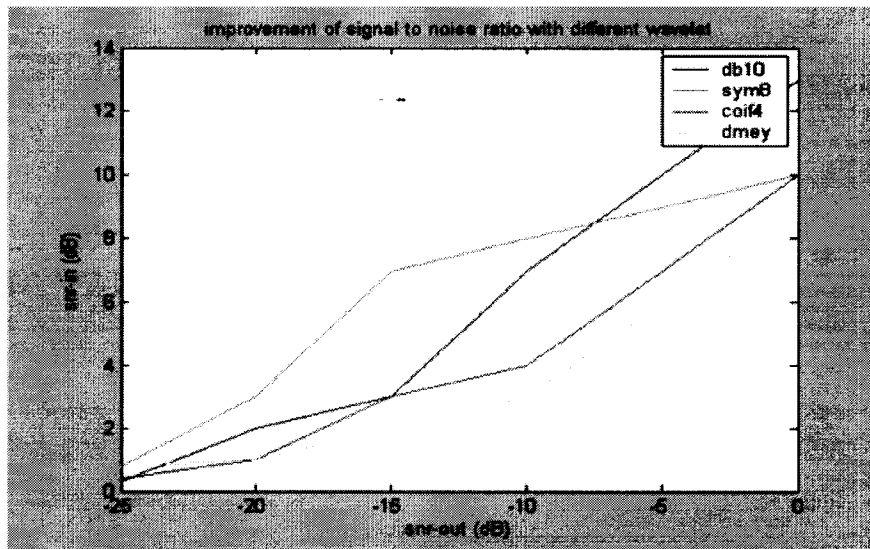
Figure 5.4-4 Improvement of SNR using different mother wavelets.

Now, the good thing in DWT that is not present in other DSP techniques used in defect detection is its capability of revealing aspects of data such as trends, breakdown points, discontinuities in higher derivatives and self-similarity. Consider the illustration below.

72

Raw signal

Denoised signal

Detail at
level 4

A-scan from real aluminum FSW sample with 4.35mm thickness
Wavelet: db10
Transducer used: Xatex, with 20 MHz frequency and 1 inch diameter
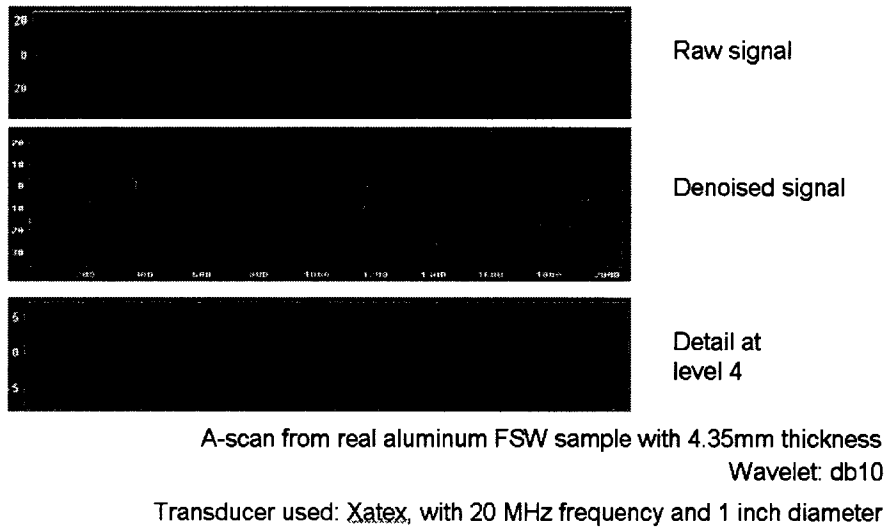
Figure 5.4-5 Raw signal, denoised signal and detail signal at level 4 using db10.

Raw signal

Denoised signal

Detail at
level 4

A-scan from real aluminum FSW sample with 4.65mm thickness
Wavelet: sym8
Transducer used: Xatex, with 20 MHz frequency and 1 inch diameter
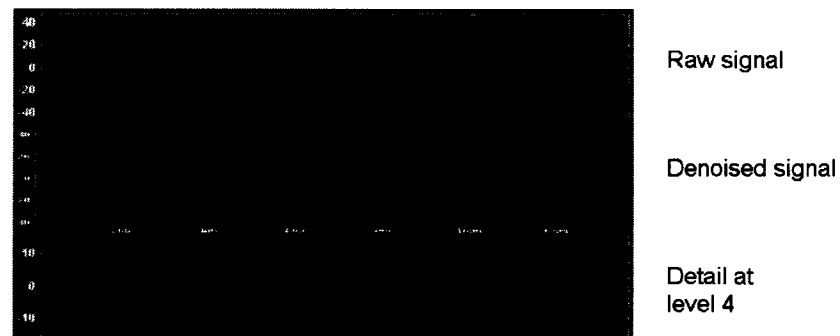
Figure 5.4-6 Raw signal, denoised signal and detail signal at level 4 using sym8.

From the noisy raw signal, DWT was able to denoise it significantly. But still, it didn't give us any interesting defect information. But once you evaluate the details at level 4, you can see that there are abrupt changes in different time locations. This might indicate the presence of flaw or defect which contains very small amount of amplitude that is probably buried in the noisy signal.

73

CHAPTER VI

CONCLUSION AND FUTURE WORKS

6.1. Conclusions

From the results, different approaches to distinguish root crack echoes from other unwanted signals acquired during ultrasound nondestructive evaluation was developed.

Due to the vertical orientation of root toe cracks, normal beam inspection is not quite effective ultrasonic NDE to apply in FSWs. From the B-scan images, it was shown that the only thing we can see is the profile of the material or some defects parallel to the scanning surface such as delaminations. Since root cracks are oriented in a different manner and location, normal beam inspection was not advisable to use, angled beam inspection was proven more appropriate. These were proven primarily with experimenting with the synthetic FSW samples. The reflections from the known flaw were easily isolated from the reflections from other parts of the specimen. The relationship of the scanning angle in angle beam inspection that can give a better signal acquisition in FSW materials was figured out. But real FSWs are far more complicated than the simple synthetic sample so more experiments were done to try and analyze if a root crack is detectable or not or just even if it is present or not.

It was proven that single element probe and phased array probe are both sensitive enough in detecting root cracks in FSWs. Array inspection provides better signal to noise ratio than single element inspections and has easier and faster manipulation. The three kinds of transducers used where all capable of detecting cracks depths as small as $50\mu m$.

74

These proved that these ultrasonic techniques were sensitive enough to detect micro crack such as root crack but with some limitations. With these limitations comes the help of signal processing techniques. Identifying root crack response from other pulses was realized in the A-scan by analyzing the responses' time of flights in either type of ultrasonic testing. From the results reported herein, by application of Discrete Wavelet Transform, detection of root cracks that are hiding from some other sources of reflection echoes was proven possible by observing that DWT results give higher signal to noise ratio after denoising. Daubechies 10, Coiflet 4, Symlet 8, and Dmey 8 are some of the most effective mother wavelet to use in these kinds of wavelet denoising.

Finally, I therefore conclude that with the use of proper ultrasonic method and with the help of wavelet noise suppression, noisy signals or unwanted signals acquired from friction stir welds will be enhanced and detection of micro cracks such as root cracks will be better, easier and more reliable.

6.1. Future Works

For future works, I recommend using an automated phased array scanning system to provide a more credible, stable signal and to have an improvement in inspection speed. Plus, it will also be helpful to expand the vitality of wavelet noise suppression into 2-dimensional analysis such as B-scan images and S-scan images. Also, it will be a great contribution if a new wavelet will be created that will give an optimal output in detection of root cracks.

REFERENCES

1) Kinchen, David and Aldahir, Esma, "NDE of Friction Stir Welds in Aerospace Application", *Inspection Trends,* July 19, 2006.

2) Ciorau,Petru, "Contribution to Detection and Sizing Linera Defects by Conventional and Phased Array Ultrasonic Techniques", *16th World Conference on NDT,* August 30, 2004.

3) Connor, Leonard, "The Welding Handbook" Volume 1, American Welding Society, Miami Florida, 1991.

4) Friction Stir Welding at TWI. Online. 2006. http://www.twi.co.uk/j32k/unprotected/band_1/fswintro.html

5) The Welding Institute Resources, Friction Processes. Online. 2005. <www.twi.co.uk>

6) Lamarre, Andre and Moles, Michael, "Ultrasound Phased Array Inspection Technology for the Evaluation of Friction Stir Welds", *15th World Conference of NDT,* October 2000.

7) Blitz, J., "Fundamentals of Ultrasonics", Butterworth and Co. Ltd., 1963.

8) Basic Principles of Ultrasonic Testing, Online. <http://www.ndt-ed.org/EducationResources/CommunityCollege/Ultrasonics/Introduction/description.htm>

9) Halmshaw, R. "Non-Destructive Testing" 2nd Edition, Great Britain, 1991.

10) McIntire, P., Green, R., and Birks, A., "Non-destructive Testing Handbook" 2nd Edition, Vol. 7, Ultrasonic Testing, 1991.

11) Olympus NDT. Online. <http://www.olympusndt.com/data/File/panametrics-UT.pdf>

12) David, J., Cheeke N., "Fundamentals and Applications of Ultrasonic Waves". CRC Press. 2002.

13) Tittman, B., and Miyasaka, C., "Scanning Acoustic Microscopy", Pennsylvania State University.

14) Inoho, Masahiro, "Resolution of Scanning Acoustic Microscope in Sub-Surface Imaging" , *Japanese Journal of Applied Physics, Vol. 27, No. 5,* May 1988, pp. 734-737.

15) Moles, M., *et.al,* "Introduction to Phased Array Ultrasonic Technology Applications", R/D tech. Inc. 2004.

16) Gebhardt, W., "Improvements of Ultrasonic Testing by Phased Arrays", *Nuclear Engineering and Design Vol. 76,* 1983. pp 275-283.

17) Wooh, Shi-Chang and Shi, Yijun, "Optimization of Ultrasonic Phased Arrays", *Review of Progress in Quantitative Nondestructive Evaluation,* New York, 1998, pp883-890.

18) Azar, L., Shi, Y., Wooh, S., "Beam Focusing Behaviour of Linear Phased Array", *NDT &E International 33,* 2000. pp.189-198.

19) Bilgutay, Nwehouse and Furgason, "Flaw visibility enhancement by split-spectrum processing techniques", *Proceedings in IEEE Ultasonic Symposium,* 1981, pp. 152-157.

20) Li, Bilgutay and Murthy, "Spectral Histogram Using the Minimization Algorithm – Theory and Applications to Flaw Detection", *IEEE Transactions on Ultrasonicss, Ferroelectrics and Frequency Control, Vol. 39, No.2,* March 1992.

21) Abbate, Koay, Frankel, Schroeder and Das, "Signal Detection and Noise Suppression Using a Wavelet Transform Signal Processor: Application to Ultrasonic Flaw Detection", *IEEE Trans. On Ultrasonics, Ferroelectrics and Frequency Control, Vol.44 No.1,* January 1997.

22) Stark, H., "Wavelets and Signal Processing", An application-based Introduction, Springer, 2005.

23) Oruklu, Erdal and Saniie,Jafar, "Ultrasonic Flaw Detection Using Discrete Wavelet Transform for NDE Applications", *IEEE Ultrasonics Symposium*, 2004.

24) Cheng, Tsukada and Hanasaki, "A novel Denoising Approcah Based On Multiresolution Thresholding and its NDT Application", *Review of Quantitative Nondestructive Evaluation Vol. 23*, 2004, pp.636-642.

25) Graville, Brian, "The Principles of Cold Cracking Control in Welds", Dominion Bridge Co. Ltd., Montreal, 1975.

26) Antoniou, Andreas, "Digital Filters: Analysis, Design and Applications", McGraw Hill Companies, 2000.

27) Tohyama, Mikio and Koike Tsunehiko, "Acoustic Signal Processing", Academic Press, 1998.

28) Pain, H.J., "Physics of Vibrations and Waves", John Wiley and Sons Ltd., 1999.

29) Etter, D. And Kuncicky, David, "Introduction to Matlab 7", Prentice Hall, 2005.

30) Kino, G.S., "Acoustic Waves: Devices, Imaging and Analog Signal Processing", Prentice Hall Inc., NJ, 1987.

31) Briggs, Andrew, "Acoustic Microscopy", Oxford, 1992.

32) Thompson, Donald et al., "Review of progress in NDE 21A", 2002.

33) Thompson, Donald et al., "Review of progress in NDE 22A", 2003.

34) Thompson, Donald et al., "Review of progress in NDE 23A", 2004.

35) Mallat, Stephane, "Theory for Multiresolution Signal Decomposition: The Wavelet Represenataion", *IEEE Transactions on Pattern Analysis and Machine Intelligence,* July 1989.

36) Ohno, M., "Resolution of Scanning Acoustic Microscope in Sub-surface Imaging", *Japanese Journal of Applied Physics,* May 1988, pp. 734-737.

37) Kino, G. "Fundamentals of Scanning Systems", Academic Press, 1981, pp. 1-21.

38) Steinberg, "Principles of Aperture and Array System Design", New York, 1976.

39) <www. Mathworks.com>

40) Krautkramer, J., "Ultrasonic Testing of Materials", New York : Springer-Verlag, 1969.

41) Dizon, Kathleen R., Titov, S., and Maev, Roman, "Detectability of Root Cracks in Friction Stir Welds with Ultrasound Inspection", *International Congress on Ultrasonics*, Vienna, Austria, April 2007.

42) Dizon, Kathleen R., Titov, S., and Maev, Roman, "Signal Processing Techniques for Enhancing Micro Crack Responses in Nondestructive Evaluation of Friction Stir Welds", *International Conference for American Society of Nondestructive Testing*, Michigan, May 2007.

KATHLEEN R. DIZON

EDUCATION

Ma. Sc. Electrical and Computer Engineering

University of Windsor, Canada

B.S. Electronics and Communications Engineering

University of the City of Manila, Philippines

ACHIEVEMENTS

Internal Academic Scholarship Awardee
University of Windsor, Canada
Winter Term 2006 to Present

Licensed Electronics and Communication Engineer
Manila, Philippines (December 6, 2005)
Registered ECE # 0033471

Academic Scholarship Awardee
University of the City of Manila, Philippines
June 1999-March 2004

RESEARCH INTERESTS
Digital Signal Processing
Phased Array Technology (R/D Tech OMNISCAN)
Sonix Acoustical Microscopy
Universal Microscopy Version 316-3 Software for NDE

PUBLICATIONS

K. Dizon, S. Titov, R. Maev, *Detectability of Root Toe Cracks in Friction Stir Welds with Ultrasound Inspection*, International Conference for Ultrasonic, April 9-12, 2007

K. Dizon, S. Titov, R. Maev, *Signal Processing Techniques for Enhancing Micro-Crack Responses in the Nondestructive Evaluation of Friction Stir Welds*, ASNT Automotive Industry Advancements with NDT Topical Conference (2007)

WORK HISTORY

Conservation and Distribution Engineer (August 2007 - Present)
St. Thomas Energy Inc.

Graduate-Teaching Assistant (January 2006-Present)
University of Windsor – Electrical Engineering Department

Research Assistant (June 2005-Present)
Dr. Roman Maev, Supervisor, Physics Department
University of Windsor

81